iScience

CellPress

Article

Human Intestinal Morphogenesis Controlled by Transepithelial Morphogen Gradient and Flow-Dependent Physical Cues in a Microengineered Gut-on-a-Chip

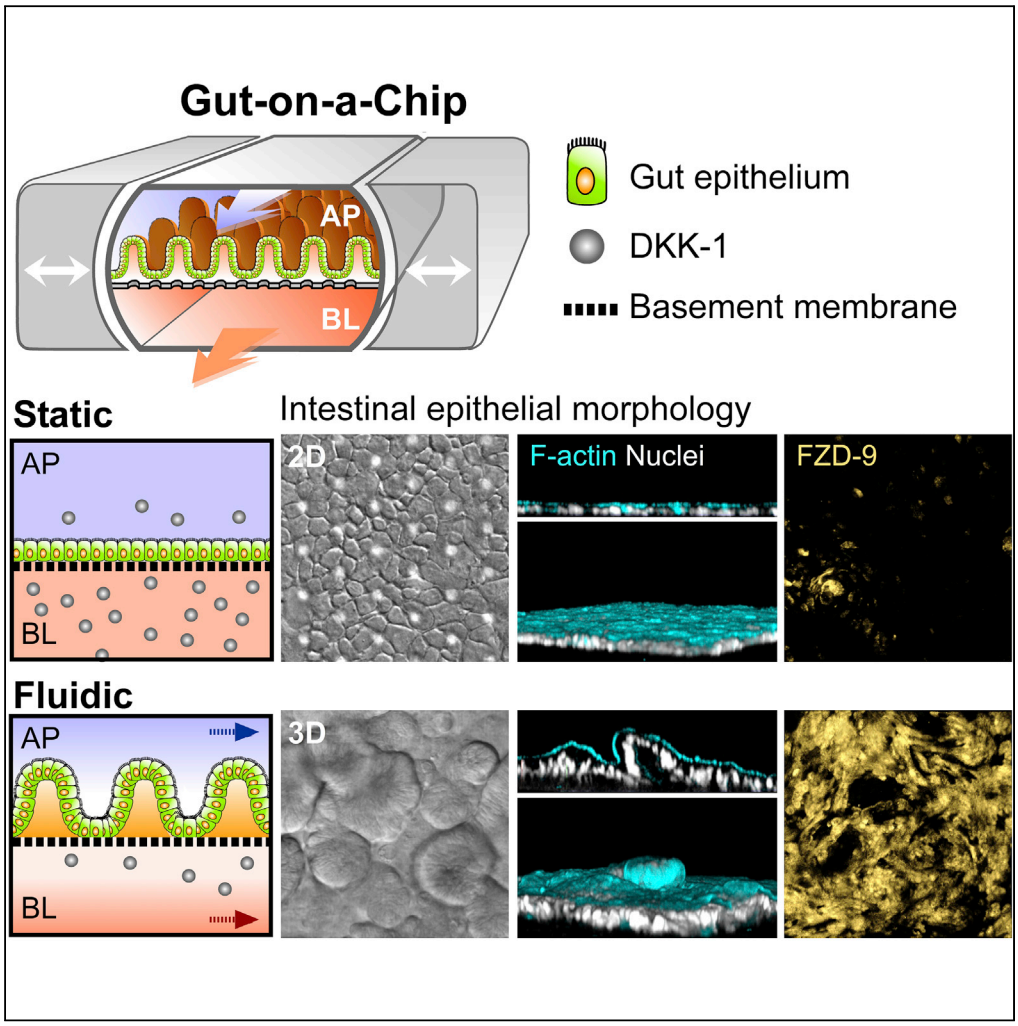

Woojung Shin, Christopher D. Hinojosa, Donald E. Ingber, Hyun Jung Kim

hyunjung.kim@utexas.edu

HIGHLIGHTS

A human Gut Chip enables one to discover the mechanism of intestinal morphogenesis

Basolateral removal of Wnt antagonist Dickkopf-1 induces villi-like morphogenesis

Flow-dependent expression of Frizzled-9 contributes to forming villi-like epithelium

Both a cell line and a primary human epithelium reproduce morphogenesis *in vitro*

Shin et al., iScience *15*, 391–406
May 31, 2019
https://doi.org/10.1016/j.isci.2019.04.037

iScience

CellPress

Article

Human Intestinal Morphogenesis Controlled by Transepithelial Morphogen Gradient and Flow-Dependent Physical Cues in a Microengineered Gut-on-a-Chip

Woojung Shin,[1] Christopher D. Hinojosa,[2,7] Donald E. Ingber,[2,3,4] and Hyun Jung Kim[1,5,6,8,*]

SUMMARY

We leveraged a human gut-on-a-chip (Gut Chip) microdevice that enables independent control of fluid flow and mechanical deformations to explore how physical cues and morphogen gradients influence intestinal morphogenesis. Both human intestinal Caco-2 and intestinal organoid-derived primary epithelial cells formed three-dimensional (3D) villi-like microarchitecture when exposed to apical and basal fluid flow; however, 3D morphogenesis did not occur and preformed villi-like structure involuted when basal flow was ceased. When cells were cultured in static Transwells, similar morphogenesis could be induced by removing or diluting the basal medium. Computational simulations and experimental studies revealed that the establishment of a transepithelial gradient of the Wnt antagonist Dickkopf-1 and flow-induced regulation of the Frizzled-9 receptor mediate the histogenesis. Computational simulations also predicted spatial growth patterns of 3D epithelial morphology observed experimentally in the Gut Chip. A microengineered Gut Chip may be useful for studies analyzing stem cell biology and tissue development.

INTRODUCTION

Understanding how local gradients of morphogens and their antagonists regulate tissue development remains a fundamental question in developmental biology (Logan and Nusse, 2004; Petersen and Reddien, 2009; Zallen, 2007), and elucidation of these mechanisms could lead to new approaches to stem cell engineering and regenerative medicine (Clevers et al., 2014). Intestinal development is a classic example whereby intestinal villus morphogenesis is known to be controlled by polarized gradients of the morphogens, but the precise physical mechanism remains unknown. For example, Wnt ligands produced by Paneth and mesenchymal cells (Farin et al., 2012) stimulate intestinal epithelial proliferation, whereas bone morphogenetic protein represses Wnt signaling and promotes cytodifferentiation as well as apoptosis as they move vertically along the crypt-villus axis (Biswas et al., 2015; Martini et al., 2017; Sato and Clevers, 2013). However, Wnt antagonists, such as Dickkopf-1 (DKK-1), are known to inhibit Wnt/β-catenin signaling (Bafico et al., 2001), and it remains unclear how all of these factors interact with each other to maintain intestinal homeostasis *in vivo*.

It has not been possible to dissect the mechanism by which the morphological three-dimensional (3D) formation of epithelium occurs in the human intestine under controlled conditions because it is difficult to recreate the localized gradient of morphogens and their antagonists in conventional static cell culture models. Intestinal organoids derived from intestinal crypts or single intestinal stem cells have been used to study crypt regeneration and crypt-epithelial domain formation *in vitro* (Farin et al., 2016; Sato et al., 2009, 2011). However, the localized morphogen gradients that drive crypt formation are randomly organized in organoid cultures, and thus, it is impossible to dissect the molecular and biophysical mechanisms that orchestrate the regulated morphogenesis. Therefore, there is a critical need for physiological tissue models that can control spatiotemporal gradients of morphogens and their antagonists with a defined developmental axis in a human organ-relevant context.

Human Organ-on-a-Chip (Organ Chip) technology, which involves the development of microfluidic cell culture devices that recreate the physical and biochemical microenvironment of key functional units of living human organs, offers an alternative approach to study intestinal structure and function. We previously

[1]Department of Biomedical Engineering, Cockrell School of Engineering, The University of Texas at Austin, Austin, TX 78712, USA

[2]Wyss Institute for Biologically Inspired Engineering at Harvard University, Boston, MA 02115, USA

[3]Vascular Biology Program and Department of Surgery, Boston Children's Hospital and Harvard Medical School, Boston, MA 02115, USA

[4]Harvard John A. Paulson School of Engineering and Applied Sciences, Harvard University, Cambridge, MA 02138, USA

[5]Department of Oncology, Dell Medical School, The University of Texas at Austin, Austin, TX 78712, USA

[6]Department of Medical Engineering, Yonsei University College of Medicine, Seoul 03722, Republic of Korea

[7]Present address: Emulate, Inc. 27 Drydock Avenue, Boston, MA, USA

[8]Lead Contact

*Correspondence: hyunjung.kim@utexas.edu

https://doi.org/10.1016/j.isci.2019.04.037

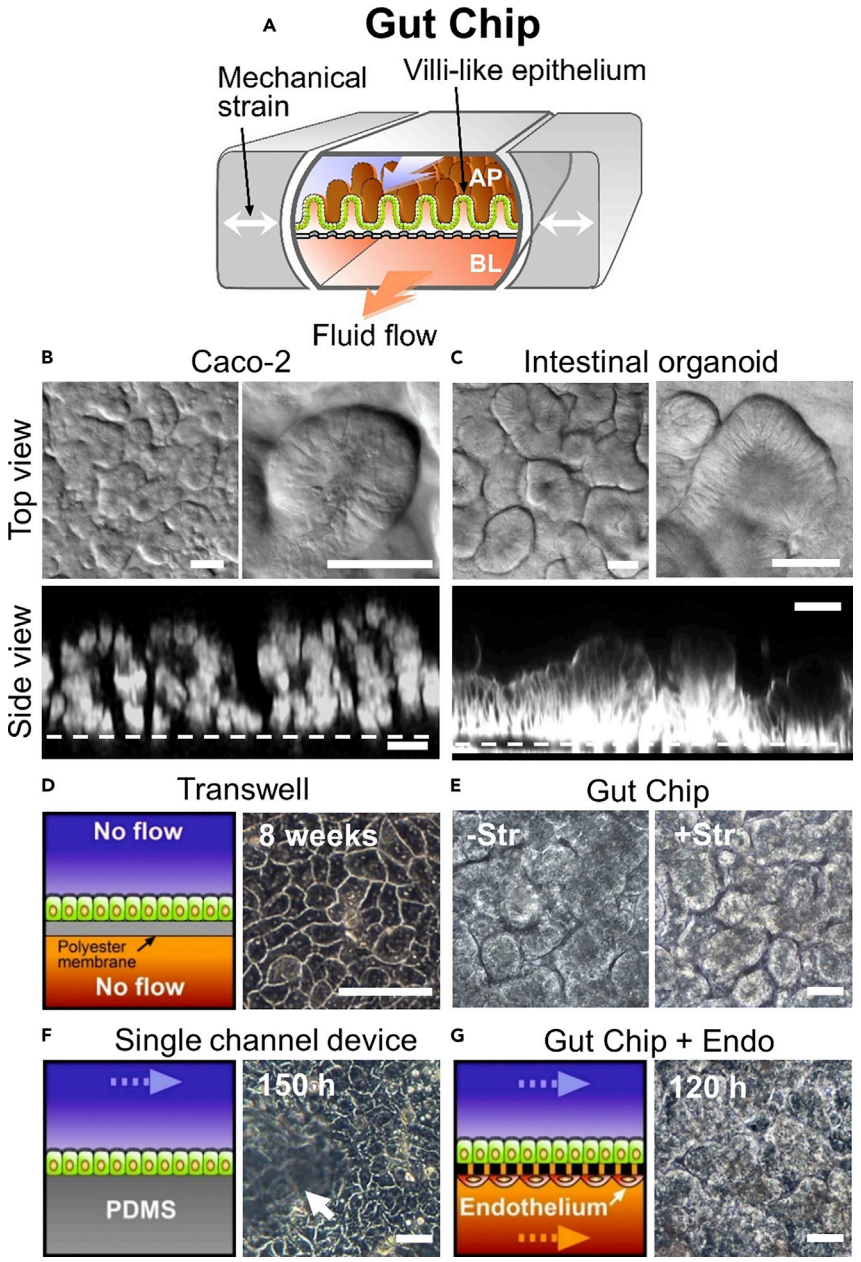

Figure 1. A Human Gut Chip Model of Intestinal Morphogenesis

(A) A schematic of the microfluidic Gut Chip containing villi-like intestinal epithelial cells adherent to the upper surface of the flexible, porous, ECM-coated membrane in the top channel of the Gut Chip (light blue and orange arrows indicate flow directions in the upper and lower microchannels, respectively; white arrows indicate mechanical deformations through application of cyclic suction).

(B) Differential interference contrast (DIC) microscopic top-down views at low (top left) and high magnification (top right) and a fluorescence microscopic cross-sectional view highlighting the nuclei (bottom; DAPI) of intestinal villi-like microarchitecture that formed spontaneously when the Caco-2 epithelium was exposed to continuous flow (30 μL/h) in both channels and cyclic mechanical strain (10%; 0.15 Hz) for approximately 100 h.

(C) Human primary organoid-derived 3D epithelial growth in a Gut Chip. DIC microscopic top-down views at low (top left) and high magnification (top right) and a vertical cross-sectional view of 3D epithelial layer fluorescently visualized the plasma membrane (bottom).

(D) A schematic diagram (left) and a phase contrast view (right) of a planar monolayer of Caco-2 cells cultured in a static Transwell insert for 8 weeks.

Figure 1. *Continued*

(E) Phase contrast views showing the villi-like morphogenesis after 96 h regardless of the absence (−Str) or the presence (+Str) of cyclic mechanical strain under continuous flow in both microchannels (30 μL/h).

(F) A schematic diagram (left; an arrow indicating the fluid flow) and a phase contrast view (right) of Caco-2 cells grown on a single-channel microfluidic device without mechanical strain in the presence of flow and apical shear stress (0.02 dyne/cm^2) for 150 h. A white arrow indicates a dome formed in the cell monolayer.

(G) A schematic diagram (left) and a phase contrast view of the epithelium in a Gut Chip in which human microvascular endothelial cells ("Endo") were pre-cultured on the opposite side of the membrane from the Caco-2 intestinal epithelial cells in the lower channel to block access of fluid shear stress (30 μL/h) to the basolateral surface of the epithelium without mechanical deformations. The schematic diagram depicts the experimental setup at the point of the co-culture that both endothelium and epithelium independently formed a monolayer.

Scale bars, 50 μm.

described a Gut Chip device lined by an intact monolayer of human Caco-2 intestinal epithelium, which spontaneously forms intestinal villi-like 3D structures when cultured under continuous flow and cyclic peristalsis-like mechanical deformations (Kim et al., 2012; Kim and Ingber, 2013). These microengineered villi-like epithelial cells recreate all four differentiated cell types of the small intestine (absorptive, goblet, enteroendocrine, and Paneth) and contain proliferative cells limited to their basal crypts. This 3D epithelium also exhibits physiological migration of proliferative cells from the crypt to the villus tip, formation of a specialized apical brush border, augmented barrier function, increased drug-metabolizing cytochrome P450 activity, and enhanced mucus production relative to static cultures (Kim et al., 2012; Kim and Ingber, 2013). In addition, the microfluidic Gut Chip model has been used to co-culture anaerobic commensal or pathogenic gut microbiome with living human intestinal epithelium for extended periods and to recapitulate the pathophysiology of intestinal inflammation and small intestinal bacterial overgrowth *in vitro* (Kim et al., 2016; Shin et al., 2019). The genome-wide transcriptome analysis confirmed that Caco-2 cells also exhibit a highly differentiated intestinal epithelial phenotype similar to that shown by the normal human ileum when cultured in the Gut Chip (Kim et al., 2016), even though the Caco-2 cells were originally isolated from human colorectal cancer that show truncating mutations in adenomatous polyposis coli (APC) tumor suppressor and β-catenin proteins (De Bosscher and Nicolas, 2004; Ilyas et al., 1997). By leveraging the Gut Chip, we also identified that the epithelial barrier dysfunction is the culprit trigger that initiates the onset of intestinal inflammation under complex host-microbiome cross talk (Shin and Kim, 2018). Formation of villi-like structures by Caco-2 cells also was previously observed by another group (Pusch et al., 2011), although their structure and function were not fully characterized. Thus, the mechanism of this epithelial morphogenesis remains unknown.

The Gut Chip is a two-channel microfluidic device that contains human intestinal epithelial cells cultured on one surface of a porous membrane that separates the channels, which makes it possible to independently control the fluid flow in each channel and to establish molecular gradients across the epithelium. As Wnt signaling is known to mediate intestinal villus morphogenesis, and Caco-2 cells secrete both Wnt molecules (Munemitsu et al., 1995; Voloshanenko et al., 2013) and the Wnt-antagonist DKK-1 glycoprotein (Koch et al., 2009; Saaf et al., 2007), we explored whether the human Gut Chip can be used to analyze how gradients of Wnt agonists and antagonists interplay to promote intestinal morphogenesis under controlled conditions *in vitro*. Also, we extended this work to the Gut Chips lined by primary intestinal epithelial cells originated from biopsy-derived intestinal organoids to confirm the physiological relevance of our findings.

RESULTS

Basal Fluid Flow Is Crucial for Intestinal Epithelial Morphogenesis

The Gut Chip is a microfluidic cell culture device composed of transparent silicone polymer (polydimethylsiloxane) that contains two apposed hollow microchannels separated by a flexible, extracellular matrix (ECM)-coated, porous membrane (Huh et al., 2013; Kim et al., 2012). The channels are lined on each side by hollow chambers that are exposed to cyclic vacuum to repeatedly strain and relax the porous membrane, thereby mimicking peristalsis-like deformations (Figure 1A). As previously demonstrated (Kim et al., 2012), when human Caco-2 intestinal epithelial cells are cultured on the upper surface of the porous flexible membrane and exposed to physiological fluid flow (30 μL/h; 0.02 dyne/cm^2) and cyclic mechanical deformations (10% in cell strain; 0.15 Hz in frequency), these epithelial cells spontaneously undergo 3D intestinal morphogenesis (Figure 1B) with finger-like projections extending vertically up to ~300 μm in height after 5 to 7 days of culture (Figure S1). Importantly, human primary intestinal organoid-derived epithelial cells

also form similar structures when cultured in the Gut Chip under physiological flow and motions (Figure 1C), as demonstrated previously (Kasendra et al., 2018). On the other hand, a Caco-2 cell monolayer maintained its planar form even when analyzed for up to 8 weeks of culture (Figure 1D). Previous studies suggested that fluid flow is more important than mechanical deformations for induction of 3D morphogenesis in this system (Kim et al., 2012), and when we repeated these studies with or without cyclic mechanical strain, we confirmed that the 3D intestinal histogenesis occurs under both conditions (Figure 1E). Thus, we then focused on how perfusing fluid flow similar to that observed within the lumen of the living intestine while flowing medium below to mimic vascular or interstitial flows that exist *in vivo* (Granger, 1981), which might influence this developmental process.

We first explored whether apical shear stress due to luminal fluid flow above the epithelium is responsible for induction of the epithelial morphogenesis. To test the effect of apical shear stress independent of the basal fluid shear generated in the lower channel, we cultured the intestinal epithelium without mechanical deformation in a single channel microfluidic device. Even though these cells were cultured under fluid flow and experienced apical shear stress, they did not show 3D morphology as in the two-channel microfluidic Gut Chip (Figure 1F). Instead, they grew as an epithelial monolayer with occasional epithelial domes being observed, as previously described in other static Caco-2 cell cultures (Ramond et al., 1985). Another possibility is that application of fluid shear stress to the basal surface of the Caco-2 cells could drive formation of the villi-like 3D structure given that the central membrane contains multiple large pores (10 μm in diameter). However, when we co-cultured the epithelial cells with capillary endothelial cells pre-grown on the surface of the porous membrane in the lower microchannel to eliminate the direct basal mechanical signal (Figure S2), Caco-2 cells continued to form 3D morphology in the upper channel in the absence of mechanical deformations (Figure 1G). Thus, application of fluid shear stress to neither the apical nor the basal surfaces of the intestinal epithelium is responsible for inducing 3D villi-like morphogenesis.

Next, we explored the possibility that the presence of continuous fluid flow might remove secreted molecules, such as Wnt antagonists, which have been reported to suppress villi formation in the past *in vitro* and *in vivo* studies (Kuhnert et al., 2004; Pinto et al., 2003). Interestingly, when we flowed medium simultaneously through both the upper and lower channels (Figure 2A, left), or through the lower channel alone while maintaining a static epithelial cell culture in the upper channel (Figure 2A, middle), 3D morphogenesis progressed normally; however, it took approximately 1.5 times longer to form villi when fluid was only flowed through the basal channel. In contrast, when the experimental protocol was reversed and fluid was only flowed above the epithelium in the upper channel, this epithelial morphogenesis was completely inhibited (Figure 2A, right).

One explanation for these observations is that the intestinal epithelial cells might secrete a certain type of inhibitory factor in a polarized manner causing it to concentrate in the lower basal channel and thereby feedback via basal membrane receptors to inhibit villi-like epithelial growth. To verify this hypothesis, we collected the conditioned medium from the basolateral side of Caco-2 cells grown for 3 days in Transwells, and then flowed this conditioned medium into the lower microchannel of the Gut Chip while fresh culture medium was flowed through the apical channel. Surprisingly, the introduction of the basally collected conditioned medium completely inhibited the 3D morphogenesis of Caco-2 cells in the Gut Chip (Figure S3). Moreover, when we cultured the Caco-2 cells on both sides of the same porous membrane, the formation of the villi-like structure was also suppressed in both microchannels (Figure S4). Taken together, these results suggest that the Caco-2 intestinal epithelial cells may secrete inhibitory factors basally that potentially antagonize the 3D morphogenesis of Caco-2 cells.

To further investigate this mechanism, we designed a hybrid device (Figure S5) that holds a Transwell insert and basally is in contact with a lower microfluidic channel that continuously removes epithelial secretomes released into the basal chamber of the Transwell. After Caco-2 cells were grown as a planar monolayer under the static condition for 3 weeks in a Transwell (Figure 2B, left), the Transwell setup was transferred to the hybrid microfluidic device. While the Caco-2 monolayer was maintained without flow apically, the medium was continuously flowed in and out (30 μL/h) through the basal microfluidic chamber, where we observed a rapid formation of 3D morphogenesis within 48 h (Figure 2B, middle). Moreover, this structural formation was similarly induced in the static Transwell inserts by simply diluting the basal medium by >100-fold in volume (Figure 2B, right), which was accomplished by placing the Transwell insert (0.33 cm^2 in surface area) in a larger culture dish containing 70 mL of static basal culture medium for 120 h. Importantly, we also

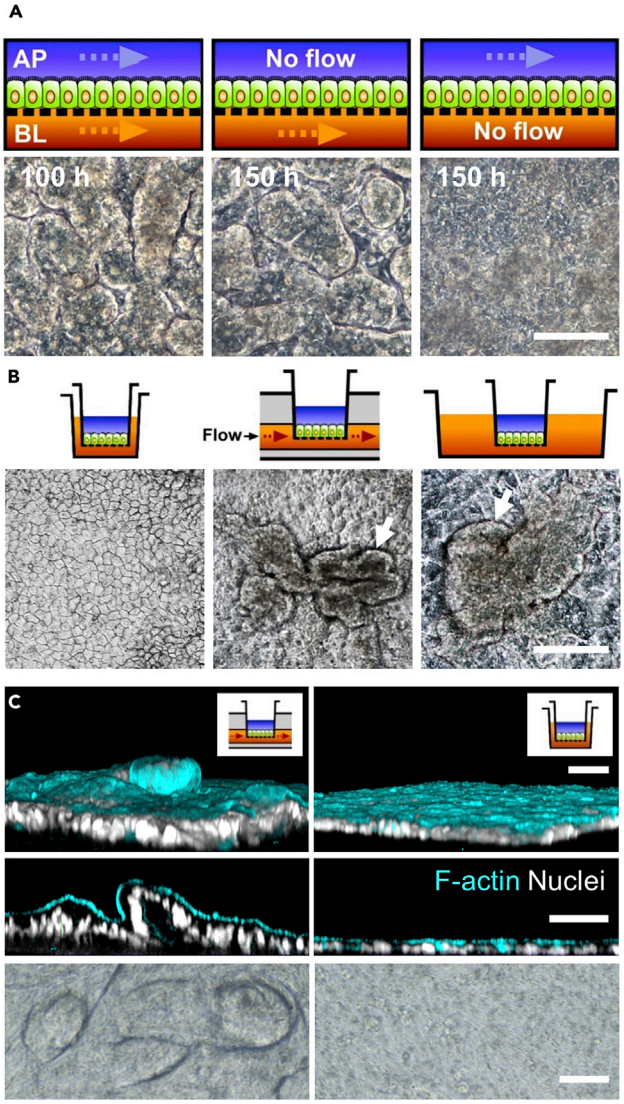

Figure 2. Basal Flow and Removal of Polarized Secreted Molecules from the Epithelium Are Necessary for Intestinal Morphogenesis

(A) Diagrams (top) and phase contrast images (bottom) of villi-like epithelium when culture medium flowed (30 μL/h) through both upper and lower microchannels (left) or only through the basal channel with no flow in the apical microchannel (middle), but not when fluid flow was stopped in the basal channel with flow continuing in the top channel (right).

(B) Schematics (top) and DIC views (bottom) showing that a planar Caco-2 monolayer cultured in a Transwell for 3 weeks can be induced to form villi-like protrusion (white arrow) by transferring the Transwell insert to a hybrid microfluidic device and applying constant flow (30 μL/h) in the basal chamber for the next 48 h (middle) or to a larger static culture well containing excess medium (70 mL) to dilute factors contained within the basal chamber for 120 h to sufficiently diffuse out basolaterally released secretomes (right). The intestinal epithelium remains as a planar monolayer in the static Transwell even after culture for up to 6 weeks (left).

(C) A monolayer of human intestinal organoid-derived epithelium pre-cultured in a Transwell insert underwent 3D morphogenesis when setup was transferred into the hybrid microfluidic device (left), whereas the same organoid-derived epithelium maintains a planar monolayer in the static condition (right). Inset schematics show the experimental setups. Cyan, F-actin; white, nuclei.

Scale bars, 50 μm.

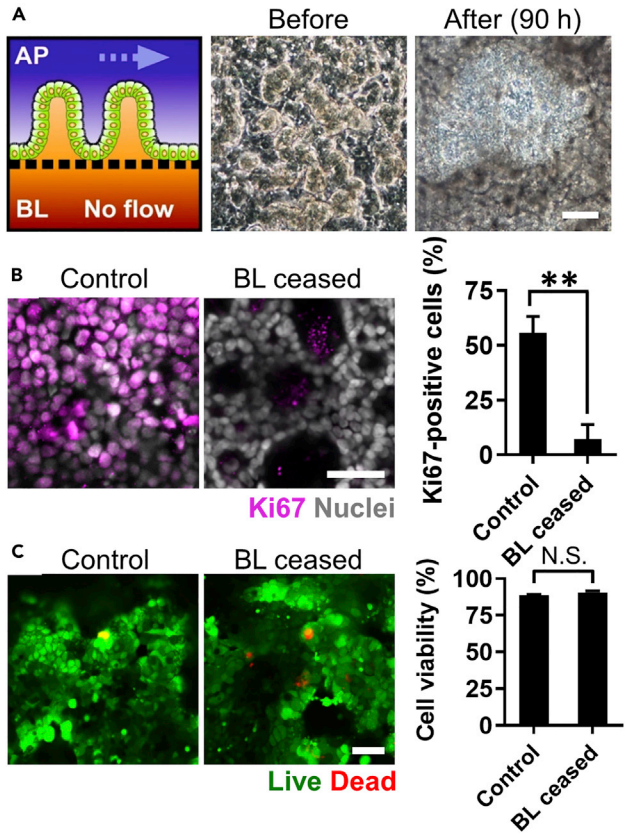

Figure 3. Cessation of Basal Flow Decreases Population of Proliferative Cells but Maintains Cell Viability

(A) A schematic (left) and phase contrast micrographs showing that the Caco-2 villi-like structure pre-formed within a Gut Chip device for ~100 h ("Before") lost the microarchitecture when basal flow in the lower channel was ceased for 90 h ("After").

(B) Visualization of the proliferative Ki67-positive Caco-2 cells (magenta) in the absence ("BL ceased") or the presence ("Control") of basolateral flow in the Gut Chips (left, middle). Quantification of the Ki67-positive cells normalized by the total number of nucleated cells (gray) (right, N = 5).

(C) Viability of Caco-2 epithelium cultured in the absence ("BL ceased") or the presence ("Control") of basolateral flow in the Gut Chips, assessed by staining with Calcein AM (Live, green) and ethidium homodimer-1 (Dead, red), and quantification of cell viability (right, N = 10). The basal flow was ceased for 48 h after 3D villi-like structure was formed in the Gut Chips by culturing for ~100 h.

N.S., not significant, **$p < 0.001$; scale bars, 50 μm.

replicated this 3D histogenesis response using primary intestinal epithelial cells derived from human intestinal organoids (Figure 2C, left), whereas a 2D monolayer of primary epithelium was maintained under static conditions (Figure 2C, right). Thus, the removal of inhibitory factors released basally by the polarized intestinal epithelium can rapidly (<2 days) trigger intestinal morphogenesis. We also observed that the cessation of basolateral flow induced the loss of pre-formed 3D epithelial microstructure within 4 days (Figure 3A). Furthermore, the number of proliferative cells labeled with Ki67 was significantly decreased under basolateral cessation of flow (<7%) compared with the control (>50%) (Figure 3B). However, a live/dead staining assay revealed that the number of dead epithelium was negligible when the basolateral flow was stopped (Figure 3C), suggesting that the loss of villi-like morphology was caused by the reduced proliferation rather than the cell death without a loss of epithelial barrier function (Figure S9B, "Control" vs. "BL ceased").

Wnt Antagonists Suppress the On-Chip Morphogenesis of an Intestinal Epithelium

Past works have shown that the canonical Wnt signaling pathway promotes villus morphogenesis in the embryonic intestine (Peifer and Polakis, 2000; Pinto et al., 2003) and human organoids (Ootani et al., 2009) via autocrine regulation. To explore whether Wnt signaling mediates the 3D histogenesis in the human Gut

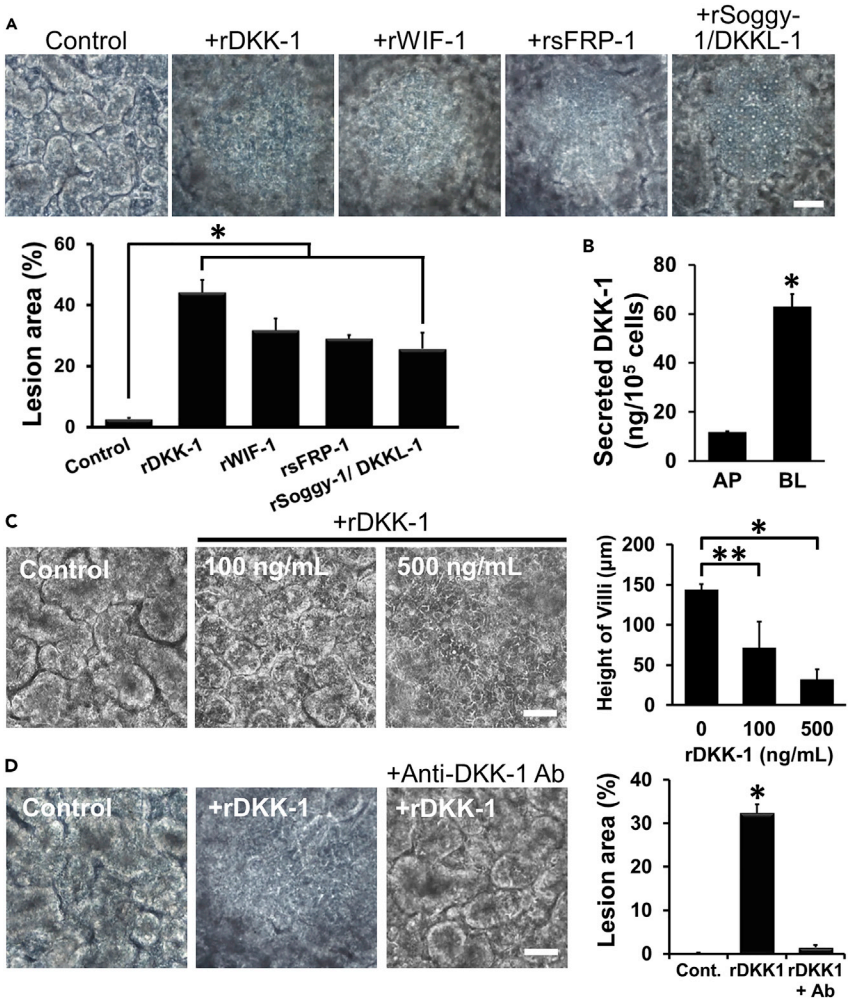

Figure 4. Wnt Antagonists Inhibit Intestinal Villous Morphogenesis

(A) Phase contrast views (top) and a graph (bottom) showing that addition of human recombinant versions of rDKK-1, rWIF-1, rsFRP-1, or rSoggy-1/DKKL-1 proteins (all at 100 ng/mL) to the medium flowing through the basal channel of the Gut Chips containing well-developed Caco-2 villi-like epithelium ("Control") resulted in the loss of 3D microarchitecture (N = 10) within 48 h.

(B) Secreted amount of DKK-1 from a Caco-2 monolayer cultured in a Transwell for 48 h (N = 3).

(C) Phase contrast views (left) and a graph (right; N = 10) showing that addition of increasing concentrations of rDKK-1 (0, 100, and 500 ng/mL) resulted in a dose-dependent suppression of the 3D epithelial morphogenesis. The culture medium containing rDKK-1 was perfused into the basolateral microchannel at 72 h since the seeding. The overall time course of villus morphology is provided in Figure S7.

(D) Phase contrast views (left) and a graph (right; N = 10) showing that the inhibitory effect of rDKK-1 (500 ng/mL) was suppressed by addition of a blocking anti-DKK-1 antibody (20 μg/mL). The rDKK-1 and anti-DKK-1 antibody were treated to villi-like epithelium for 48 h.

Scale bars, 50 μm; *p < 0.001, **p < 0.05.

Chip, we, respectively, added human recombinant Wnt antagonists including DKK-1 (rDKK-1), Wnt inhibitory factor 1 (rWIF-1), secreted frizzled-related protein 1 (rsFRP-1), and Soggy-1/DKK-like 1 (rSoggy-1/DKKL-1) (Kawano and Kypta, 2003) to the culture medium that was perfused to the lower microchannel of the Gut Chips, which had pre-formed villi-like epithelium (Figure 4A, "Control"). As expected, all of these Wnt antagonists induced the loss of 3D morphology within 48 h of the exposure (Figures 4A and S6), and the percentage of epithelial surface that exhibited the morphologically blunted lesion was significantly higher in the cultures treated with each of the Wnt antagonists compared with the control (Figure 4A, bottom).

We then selected the most potent and well-characterized antagonist, DKK-1 (Aguilera and Munoz, 2007; Gonzalez-Sancho et al., 2005), to further investigate the mechanism of inhibition. First, we confirmed that the Caco-2 cells cultured in a Transwell secrete approximately 5.3-fold more DKK-1 ($p < 0.001$) into the basal chamber than into the apical side (Figure 4B), which shows a good agreement with our observation in Figures 2 and 3. Addition of rDKK-1 to the basal channel resulted in a statistically significant ($p < 0.05$), dose-dependent reduction of the height of 3D epithelium (Figures 4C and S7). Moreover, when we analyzed the same location in the chip over time, we found that, although the presence of the rDKK-1 antagonist for 48 h resulted in the loss of villi-like structure (Figure S8A), removal of rDKK-1 resulted in the rapid restoration of epithelial 3D growth within 24 h (Figure S8B). However, the villi-like microarchitecture was involuted once again when we resumed rDKK-1 treatment for an additional day (Figure S8C). We also confirmed that the inhibition of 3D epithelial morphogenesis by rDKK-1 can be successfully suppressed by the co-treatment of an anti-DKK-1 monoclonal antibody (Figure 4D) for neutralizing the antagonistic function of DKK-1. We also confirmed a decreased population of Ki67-positive proliferative cells when the rDKK-1 was treated to Caco-2 villous epithelium for 48 h (Figure S9A), whereas the barrier integrity was well maintained (Figure S9B). Furthermore, when we added the same anti-DKK-1 antibodies to the Caco-2 monolayers grown in static Transwells (Figure S10), the average height of the cell monolayer significantly increased compared with the control (Figure S10C; $p < 0.0001$). Interestingly, nucleated cells were observed beginning to extend above the surface of the planar epithelial monolayer (Figure S10B, a zoomed-in inset), suggesting that the addition of anti-DKK-1 antibody contributed to the initiation of morphogenesis.

Computer Simulation Predicts Transepithelial Morphogen Gradient

We then built a multi-physics, finite element model of the Gut Chip to better understand how polarized secretion of Wnt antagonists and generation of the gradient of a Wnt inhibitor may contribute to the spatiotemporal control of epithelial 3D growth patterns. This simplified computational model assumes that DKK-1 is the most relevant and potent morphogen antagonist and computes the concentration of DKK-1 and Wnt within the geometry of the Gut Chip, taking into account the relative production rate of both molecules by the intestinal epithelium, diffusion through the medium, and convection due to the fluid flow. We estimated the diffusion coefficient of DKK-1 to be two orders of magnitude greater than that of Wnt based on the past work (Sick et al., 2006), which we set at 9.3×10^{-11} and 6.9×10^{-13} cm^2/sec, respectively. The production rate of DKK-1 (421 pg/10^6 cells/h) by the Caco-2 cells was applied from the previous study (Koch et al., 2009), where we postulated the same production rate for Wnt because binding of Wnt to its receptors stimulates production of both itself and DKK-1 (Sick et al., 2006). Quantitation of Caco-2 cell numbers in the Gut Chip revealed that the epithelial cell layer contains $\sim5.0\times10^5$ cells/chip ($\sim4.5\times10^6$ cells/cm^2).

We first performed the simulation to explore if the accumulated DKK-1 can form a stable gradient in the lower microchannel of a simplified 2D representation of the Gut Chip (Figure S11). Under static flow conditions (i.e., 0 μL/h), DKK-1 was simply accumulated in the basal channel; however, as flow rate is increased up to 30 μL/h, the simulation predicts that a gradient of DKK-1 molecules will be generated with lower concentrations at the bottom of the basal channel and toward the inlet. Furthermore, when the flow rate was increased above 50 μL/h, the model predicted that DKK-1 levels would fall to almost zero in the lower channel.

We then used a more complex 3D model to analyze the concentration of DKK-1 along the length and width of a perfused channel in the Gut Chip, assuming that the polarized cells are secreting DKK-1 from their basolateral surface. This model predicted that the concentration of DKK-1 near the inlet of the microchannel would be relatively low, whereas the level of DKK-1 will increase by 10-fold or more near the channel outlet (Figures 5A and S12). Interestingly, when we experimentally analyzed villus growth at 80 h in regions corresponding to the upstream, middle, and downstream positions in the microchannel (Figure 5A), we observed that there was a gradient of pseudo-villous growth that closely mirrored the pattern predicted by the computational model. For example, vigorous 3D morphogenesis was observed in the upstream region, whereas the least formation of the villi-like structure was found in the downstream portion in the microchannel (Figure 5B). The 3D computational model also predicted a parabolic distribution of DKK-1 accumulation at the surface of the porous ECM-coated membrane, with lower concentrations in the center of the channel and higher concentrations near the sidewalls of the channel (Figures 5A and S12). This result is attributed to the parabolic profile of laminar flow in the microchannel, where the linear flow velocity will

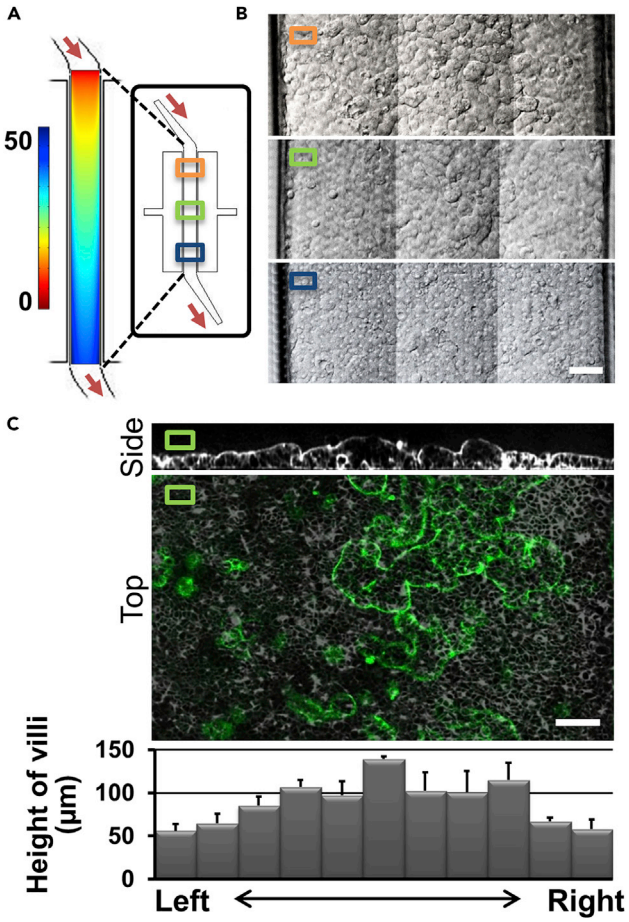

Figure 5. The Spatiotemporal Pattern of Villi-like Epithelial Structure Is Governed by the Gradient of Morphogen Antagonists

(A) A computational simulation based on the results shown in Figure S11 displaying the spatial pattern of DKK-1 concentrations at the bottom surface of the membrane under the flow (30 μL/h) mapped on a schematic of a Gut Chip, indicating that it will form a parabolic gradient and exhibit a gradient of concentration levels with lowest near the inlet and highest downstream near the outlet. Color bar, the scaled range of DKK-1 concentrations (unit, $\times 10^{-9}$, mol/m^3). An inset at the right shows the structure of a Gut Chip, where the orange, green, and blue boxes overlaid on the device design at the right indicate the location of up-, mid-, and downstream snapshots of the microchannel shown in (B); red arrows indicate the flow direction.

(B) Stitched DIC images showing that growth patterns of the Caco-2 villi-like epithelium along the longitudinal gradient in the corresponding up-, mid-, and downstream regions of the Gut Chip as indicated by colored squares in (A) at 80 h.

(C) Vertical cross-sectional (upper) and top (middle) views of immunofluorescence images of the Caco-2 epithelium grown on-chip for 80 h at mid-stream region shown in (A) and stained with a fluorescent membrane dye (green) to highlight the surfaces of the cells and laid over the DIC image. A graph at the bottom shows the distribution of epithelial height across the width of the microfluidic channel at the mid-stream position designated with a green box in (A–C). N = 5; scale bars, 100 μm.

be the highest in the center, therefore washing away DKK-1 at a higher rate, with DKK-1 accumulation where the flow is the lowest near the channel walls. In fact, we experimentally confirmed that the growth of 3D epithelium exhibited a similar pattern on-chip, in which both the height and abundance of the villi-like structure are higher in the middle of the channel compared with its sides near the wall where the inhibitor levels are lower (Figure 5C).

Interestingly, we experimentally observed that the intermediate flow rate regime (70–120 μL/h) resulted in faster growth of taller villi-like epithelial structure per unit time compared with flow rates below 30 μL/h or above 120 μL/h, which produced significantly slower morphogenesis (Figures 6A and S13). We then compared effects of three representative flow rates (30, 100, and 200 μL/h) in the Gut Chips versus static

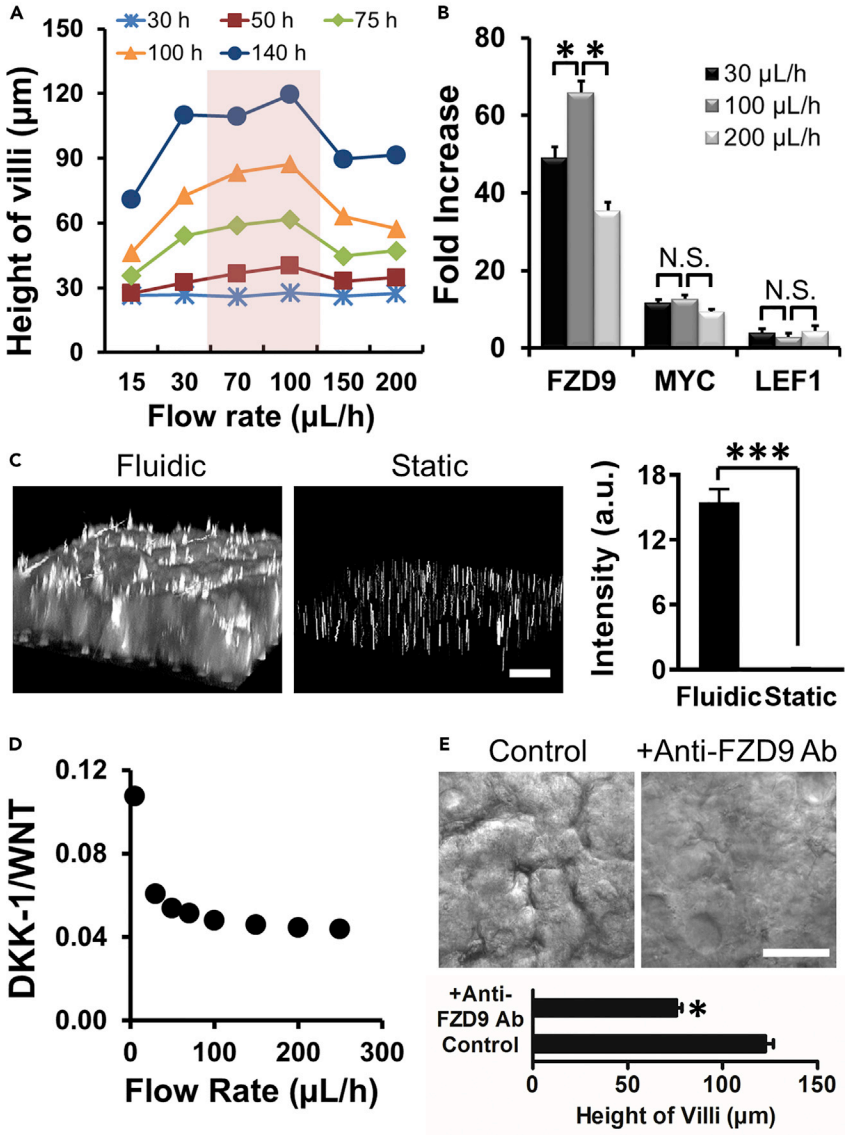

Figure 6. Mediation of Intestinal Villi-like Morphogenesis by the Wnt FZD9 Receptor

(A) A graph showing profiles of epithelial height at various flow rates (15, 30, 70, 100, 150, and 200 μL/h) over time. The highlighted region indicates the optimal flow rate regime that maximizes the formation of villi-like morphology (Error bars are smaller than the symbol size).

(B) A graph showing fold increase in expression of FZD9, MYC, and LEF1 genes in Caco-2 intestinal epithelial cells grown in the Gut Chip at different flow rates (30, 100, and 200 μL/h) compared with the static Transwell (*$p < 0.05$; N.S., not significant).

(C) Expression of FZD9 on Caco-2 villi-like epithelium in fluidic and static culture conditions, visualized by immunofluorescence imaging and 3D reconstruction of z-stacked images (left). Caco-2 cells were cultured in a Gut Chip under 30 μL/h in the fluidic condition or a 96-well plate for 100 h as a static condition. The intensity of each condition was quantitated using Image J (right) (***$p < 0.0001$; N = 5).

(D) Mathematical prediction of the ratio of DKK-1 and Wnt molecules in the Gut Chip probed at the surface of the porous membrane within the lower channel for a range of flow rates.

(E) Phase contrast microscopic views (top) and a graph (bottom) show that addition of blocking anti-FZD9 antibodies ("+Anti-FZD9 Ab"; 20 μg/mL) successfully inhibited the formation of a 3D villi-like epithelial layer and resulted in the significant decrease in epithelial height after 24 h when compared with control. (*$p < 0.01$; scale bars, 50 μm).

Transwell cultures at 48 h and performed quantitative real-time polymerase chain reactions (qPCR) targeting 92 human Wnt-related genes. The qPCR results revealed that only three genes, G protein-coupled receptor (GPCR) frizzled 9 (FZD9), Myc (MYC), and lymphoid enhancer-binding factor 1 (LEF1), were significantly ($p < 0.05$) upregulated in the Gut Chips under flow compared with Transwells. Consistent with the predictions from the computational model, the Wnt receptor FZD9 exhibited the highest and the most significant ($p < 0.01$) upregulation (~66-fold increase) at a flow rate of 100 μL/h, whereas cells in the chips exposed to lower or higher flow rates (30 or 200 μL/h, respectively) exhibited less increment in FZD9 (~49- and ~36-fold, respectively) (Figure 6B). However, there was no significant difference in MYC and LEF1 regardless of the flow rates. Immunofluorescence confocal microscopy showed that the expression level of FZD9 was significantly ($p < 0.001$) higher in the fluidic than in the static culture condition in both Caco-2 (Figure 6C) and organoid-derived epithelium (Figure S14). A computational simulation accounting for the production rates of DKK-1 and Wnt molecules at the basolateral membrane revealed that the relative ratio of DKK-1 and Wnt at the steady state is almost constant at flow rates greater than ~30 μL/h, whereas the ratio exponentially increases as flow rates approach static conditions (i.e., 0 μL/h) (Figure 6D). This result suggested that the flow-dependent 3D morphogenesis of Caco-2 cells is predominantly orchestrated by the FZD9 receptor because the DKK-1/Wnt ratio was almost constant regardless of the flow rate at >30 μL/h.

To confirm if FZD9 is a critical receptor for intestinal morphogenesis, anti-FZD9 blocking antibodies were added to the villi-like epithelium pre-established in the Gut Chip. We found that the infusion of anti-FZD9 antibodies (20 μg/mL) into both the apical and basal microchannels of the Gut Chip substantially altered the 3D morphology (Figure 6E). Epithelial height was 122.5 ± 4.2 μm in the control group, whereas it was significantly ($p < 0.05$) reduced to 75.8 ± 2.7 μm when FZD9 receptors were blocked (Figure 6E). Taken together, our finding suggests that FZD9 is a key receptor that mediates control of intestinal morphogenesis through its interactions with Wnt and DKK-1 in the microengineered model.

DISCUSSION

Our mechanistic study that leverages a microphysiological Organ Chip uncovers the molecular basis of a developmental morphogenic process *in vitro* that is governed by complex cellular signaling. The Gut Chip enabled separate access to the apical lumen and basal abluminal compartments of this engineered intestinal epithelium, as well as precise independent control over fluid flow rates, molecular components, and, hence, transepithelial gradients while allowing high-resolution microscopic imaging. By manipulating biophysical and biochemical cues in the Gut Chip, we discovered that the Wnt antagonist DKK-1 is secreted in a polarized basolateral direction and that its removal by fluid flow in the basolateral microchannel is a crucial factor that directly triggers intestinal 3D morphogenesis in this *in vitro* model using Caco-2 as well as the primary organoid-derived epithelial cells. We also discovered that the Wnt receptor FZD9 mediates this morphogenic response, where its expression level is dependent on the flow rate and correlates with epithelial differentiation. Experimental results that we obtained were verified with the computational modeling designed to understand the molecular distribution and dynamics of secretory DKK-1 and Wnt in the Gut Chip. By using a simple computational simulation, we successfully explained the morphogenic patterns of epithelial growth inside the microfluidic channel reminiscent of the intestinal development.

Our past finding that human Caco-2 intestinal epithelial cells spontaneously undergo villus morphogenesis and small-intestine-specific cytodifferentiation and histogenesis in the microfluidic Gut Chip (Kim et al., 2012; Kim and Ingber, 2013) was surprising because Caco-2 cells cultured under static conditions, or even under microfluidic flow, did not exhibit this response in prior studies. The results of the current study now explain this disparity because those past studies did not include basolateral flow (Gao et al., 2013; Imura et al., 2009). However, although fluid flow was found to be more critical than peristalsis-like deformations in triggering the formation of villi-like epithelial microarchitecture, we found that direct application of fluid shear stress to the epithelial cells is not sufficient to induce the morphogenesis in the Gut Chip. This observation suggested that fluid flow might influence histogenesis by altering the delivery or removal of soluble signaling factors. Thus, we explored whether fluid-flow-dependent changes in delivery of Wnt and removal of Wnt-antagonistic molecules such as WIF, sFRP-1, DKKL-1, and DKK-1 modulate structural changes. WIF-1 binds directly to Wnt proteins and prevents the initiation of the Wnt-signaling pathway (Malinauskas et al., 2011). sFRP-1 also binds to Wnt proteins to inhibit Wnt signaling as an antagonist (Bovolenta et al., 2008). DKKL-1, also known as Soggy-1, is a homologue to the DKK family proteins. However, DKKL-1 does not affect canonical signaling of the Wnt/β-catenin pathway, which acts differently from

DKK-1 protein (Yan et al., 2012). Regardless of their specific mechanism, all of these Wnt antagonists involuted the preformed Caco-2 villi-like structure. We further studied how the removal of Wnt antagonists mediates the intestinal morphogenesis by using DKK-1, which have been previously implicated in control of intestinal morphogenesis (Crosnier et al., 2006; Ootani et al., 2009) and are known to be produced by Caco-2 epithelial cells (Koch et al., 2009; Voloshanenko et al., 2013).

Our study revealed that the reduction of basolaterally secreted DKK-1, potentially other Wnt antagonizing molecules as well, is the crucial trigger that orchestrates the epithelial histogenesis in the Gut Chip as well as in the hybrid microfluidic device. When we removed secreted DKK-1 under either fluidic or diffusion-based conditions, 3D morphogenesis of intestinal epithelial cells was promoted. This approach was verified even in the presence of an endothelial layer at the opposite side of the porous membrane in the Gut Chip. It is noted that the endothelial layer we cultured in this experiment has a high permeability to large molecules via transcytosis (Fung et al., 2018; Mehta and Malik, 2006). Therefore, DKK-1 that are basolaterally secreted by the Caco-2 cells can be readily transported through the endothelial layer, which potentially leads to the epithelial morphogenesis.

In the normal intestinal epithelium, Wnt molecules are mainly localized on the external cell surface where they activate downstream Wnt signaling, and diffusion of Wnt molecules to adjacent epithelial cells is negligible (Farin et al., 2016). Caco-2 cells have shown a continuous activation of Wnt/β-catenin signaling because of truncating mutations in APC and β-catenin (Voloshanenko et al., 2013). Interestingly, autologous secretion of DKK-1 by Caco-2 cells concomitantly occurs in conventional Caco-2 cultures at about 42.1 pg/10^5 cells/h (Koch et al., 2009; Takahashi et al., 2010). However, it is notable that the presence of DKK-1 does not completely block the proliferation of Caco-2 cells (Koch et al., 2009), which has been confirmed in our previous and current studies. As the inhibitory DKK-1 molecules are freely secreted and bind to membrane receptors such as low-density lipoprotein receptor-related protein (LRP) 5/6 (Bafico et al., 2001), these observations are consistent with the mechanism we uncovered here, in which removal of the secreted Wnt inhibitor DKK-1 can directly initiate intestinal morphogenesis in Caco-2 epithelium. Furthermore, the presence of DKK-1 can induce disruption of intestinal villi in the *in vivo* mouse models (Kuhnert et al., 2004), which was also replicated in our current *in vitro* study (Figure 4). Although the averaged molecular weight of Wnt family members (38–42 kDa) (Gavin et al., 1990) is larger than DKK-1 (28.7 kDa) (Aguilera and Munoz, 2007), our computational model suggests that, as a consequence of production and secretion by Caco-2 cells, the ratio of DKK-1 and Wnt molecules at the steady state is almost constant at flow rates higher than 30 μL/h, suggesting that the ratio of DKK-1/Wnt is independent of flow rate. Thus, the flow-dependent profile of secreted Wnt antagonist molecules, such as DKK-1, is likely a key feature that controls the intestinal 3D morphogenesis in the Gut Chip.

We found that the cessation of basolateral fluid flow in the Gut Chip can also induce the loss of preformed villi-like microarchitecture. We hypothesized that the disappearance of 3D epithelium under the cessation of basolateral flow might result from either the increased death of cells or the decreased proliferation of cells. We discovered that the cessation of basal flow significantly decreased the number of Ki67-positive proliferative cells, whereas the control group that experienced continuous basolateral flow maintained proliferative population more than 10-fold. However, neither the cell viability nor the barrier function was compromised in response to both the cessation of basal flow and treatment of rDKK-1, suggesting that the maintenance of proliferative cell population may be a crucial element to sustain the intestinal epithelial morphogenesis and its microarchitecture over time.

The directional secretion of DKK-1 in a polarized monolayer of the human intestinal epithelium has not been reported, although secretion and antagonism of DKK-1 in Wnt/β-catenin signaling is a common developmental feature in vertebrates (Farin et al., 2012; Glinka et al., 1998). Furthermore, we also verified the 3D morphogenesis mechanistically using primary epithelial cells obtained from human intestinal organoids in the same Gut Chip as well as in the hybrid microfluidic device. Since the organoid-derived epithelial culture is constitutively supported by the high level of Wnt, R-Spondin, and Noggin (Saxena et al., 2015), it was evident that the removal of morphogen antagonists by fluid flow in the basolateral side is critical for the intestinal morphogenesis in this primary cell culture model. Although the regeneration of 3D microarchitecture of organoid-derived epithelium was previously reported using human small intestinal organoids (Kasendra et al., 2018), it has not been clear which factor triggers this epithelial morphogenesis.

The wave of rostral-to-caudal (oral-to-anal) formation of the villi during the intestine development has been long recognized (Johnson, 1910; Kammeraad, 1942; Walton et al., 2012). This proximal-to-distal wave of development results in a progressive decrease in the height of villi along the length of the intestine from duodenum to jejunum, ileum, and colon (Walton et al., 2012). Thus, the temporal growth pattern observed in the present study in which villi-like structure first emerged in the proximal (upstream) region of the Gut Chip near the inlet where their heights are also the longest, and then they progressively shorten toward the outlet, is remarkably reminiscent of what is observed during vertebrate intestine development (Spence et al., 2011). However, our results are different from those of the past *in vivo* study, which suggested that Hedgehog (HH)-dependent intestinal mesenchymal cell clusters orchestrate the patterning and generation of villi within the adjacent intestinal epithelium (Walton et al., 2012). Thus, it will be interesting to explore whether the Wnt signaling we discovered occurs *in vivo* and, if so, how it interplays with HH signaling-mediated epithelial-mesenchymal interactions. Mesenchymal cells (e.g., intestinal fibroblasts) that produce tissue-specific morphogens (Powell et al., 2011) could be potentially integrated into the Gut Chip to explore this mechanism *in vitro* in future studies.

We initially expected that the growth rate of villi-like epithelium would proportionally increase as a function of flow rate because higher flow rates should remove Wnt antagonists more efficiently. However, among six different flow rates in a range of 15-200 μL/h, the epithelial growth we observed experimentally was slower at flow rates >100 μL/h compared with the intermediate flow rate regime. This discrepancy suggested that there may be an additional factor that orchestrates the epithelial morphogenesis independently of constitutive competition between Wnt agonists and antagonists. Our qPCR analysis revealed that the expression of the Wnt receptor FZD9 significantly increased among 92 human Wnt-related genes at the intermediate-flow-rate regime compared with lower or higher rates, which correlated directly with the degree of morphogenesis. Immunofluorescence imaging revealed that the fluid flow significantly increased the expression of FZD9 receptor in both Caco-2 and human organoid-derived epithelium, suggesting that FZD9 expression is dependent on fluid flow. Moreover, blocking the upstream signaling by neutralizing FZD9 remarkably reduced the formation of villi-like structures in Caco-2 cells. We revealed that the expression of FZD9 is regulated by the fluid flow, and it represents a morphogenetic control mechanism. The function of FZD9 is poorly understood compared with other well-characterized FZD receptors (Bafico et al., 1999). Thus the use of the microfluidic human Gut Chip may help to mechanistically unravel the role of FZD9 in development and morphogenesis in the human intestine.

Intestinal morphogenesis has been promoted *in vitro* previously by culturing intestinal organoid-derived epithelial cells in the presence of Wnt (Farin et al., 2012; Sato et al., 2011), or Wnt-producing Paneth-like cells (Sato et al., 2011) or mesenchymal cells (Valenta et al., 2016). Interestingly, the cell-elaborated Wnt factors, which normally contribute to generation of localized Wnt gradients in the intestinal crypt microenvironment, induce formation of crypt-like protrusion with intervening villus domains within the crenulated organoids, whereas addition of soluble Wnt often promotes the formation of round spheroids that fail to undergo villus morphogenesis (Farin et al., 2012; Sato et al., 2009). Thus, organoids require the presence of live Wnt-producing cells to create spatiotemporal gradients of Wnt (and possibly its inhibitors as well) that are required for histogenesis, which is consistent with the importance of mesenchymal clusters observed during intestinal development *in vivo* (Walton et al., 2012). In contrast, Caco-2 epithelial cells, which were originally isolated from a tumor, secrete Wnt molecules constitutively and exhibit autocrine activation of FZD9 receptors, which may contribute to their stem cell-like behaviors as well as their ability to undergo 3D morphogenesis in the absence of mesenchymal cells. However, similar observation when primary organoid-derived human intestinal epithelial cells were cultured on-chip suggests that the removal of Wnt antagonists and the flow-dependent expression of Wnt receptors may play a pivotal role in the control of intestinal morphogenesis. Furthermore, when the organoid-derived epithelium is cultured in static, intestinal morphogenesis does not occur regardless of the presence of Wnt, R-spondin, noggin, and various growth factors (Ettayebi et al., 2016; Noel et al., 2017). Thus, our finding in this study and the prior reports strongly suggest that the demonstration of epithelial 3D morphogenesis may be predominantly driven by the removal of morphogen antagonists rather than by the addition of morphogen or the origin of cell source (e.g., cancerous vs. normal).

The current study provides an exceptional example showing how spatial control of morphogen antagonists can orchestrate epithelial morphogenesis by establishing asymmetry across the epithelial cells and sustaining differences between their apical versus basolateral microenvironments during tissue growth. This finding is consistent with the past observation that spatiotemporal morphogen gradients and control of

extracellular morphogen antagonists are as important as the type of morphogen for control of development (Kawano and Kypta, 2003). Although the Wnt gradient *in vivo* has been well characterized (Scoville et al., 2008), the gradient profile of DKK-1 *in vivo* has been insufficiently discussed (Du et al., 2013), suggesting that the power of the Organ Chip technology is that we can identify the complex mechanism by precisely controlling gradients and independently varying potential morphogenic parameters one at a time, in both time and space. This ability to control directional flow rates, fluid shear stresses, mechanical deformations, and asymmetric stimulation of the apical versus the basolateral side of a developing epithelium cannot be easily achieved in any other culture system or animal model. Thus, Organ Chips may offer a compelling *in vitro* tool to decipher cellular, molecular, and biophysical mechanisms of developmental control that underlie histogenesis of the intestine, as well as other epithelial tissues.

In summary, we discovered that human intestinal morphogenesis is controlled by a transepithelial gradient of the Wnt antagonist DKK-1 and flow-dependent induction of the Wnt FZD9 receptor using a microfluidic Gut Chip as a model system. DKK-1 is secreted asymmetrically across the epithelium resulting in higher concentrations in the basal compartment, where the presence of basal fluid flow removes this inhibitor and promotes intestinal epithelial morphogenesis. The expression of FZD9 varies with flow rate, and the location and height of Caco-2 intestinal villi-like epithelium scale directly with its expression levels. This microfluidic experimental platform can be further expanded to incorporate other cell types (e.g., mesenchymal cells) to explore how they contribute to this morphogenic response, in addition to exploring other unknown questions in developmental biology that involve the establishment of chemical gradients or variations in the local physical microenvironment.

Limitations of the Study

Caco-2 intestinal epithelium formed in the Gut Chip might not sufficiently recapitulate the normal physiology observed *in vivo*. This study was performed in the absence of other cell types such as mesenchymal cells or vascular components that may support epithelial morphogenesis in the intestinal microenvironment. For instance, myofibroblasts in the lamina propria area are known to produce morphogens and interact with the intestinal epithelium to control Wnt signaling (Roulis and Flavell, 2016). Therefore, incorporation of other tissue-specific cell types can further improve the accuracy of the Gut Chip model to study morphogenesis of intestinal epithelium *in vitro*. In addition, identification of cross talk between DKK-1 and FZD9 remains as a future study.

METHODS

All methods can be found in the accompanying Transparent Methods supplemental file.

SUPPLEMENTAL INFORMATION

Supplemental Information can be found online at https://doi.org/10.1016/j.isci.2019.04.037.

ACKNOWLEDGMENTS

This work was supported partially by Alternatives in Scientific Research of the International Foundation for Ethical Research (IFER) Graduate Fellowship (UTA15-001318 to W.S.), Bio & Medical Technology Development Program of the National Research Foundation (NRF) funded by the Ministry of Science and ICT (2018M3A9H3025030 to H.J.K.), Cancer Research Institute (UTA18-000889 to H.J.K.), Alternatives Research and Development Foundation (UTA18-001198 to H.J.K.), The Leona M. and Harry B. Helmsley Charitable Trust (Grant #1912-03604 to H.J.K.), Defense Advanced Research Projects Agency (Cooperative Agreement Number W911NF-12-2-0036 to D.E.I.), Food and Drug Administration (grant #HHSF223201310079C to D.E.I.), and the Wyss Institute for Biologically Inspired Engineering at Harvard University. The content of the information does not necessarily reflect the position or the policy of the Defense Advanced Research Projects Agency or the U.S. Government and no official endorsement should be inferred. We thank Dr. J. Lee and C. Lucchesi for their help with the qPCR analysis. We thank Dr. S. Payne (UT Austin) for providing intestinal organoids derived from normal human colonic crypts.

AUTHOR CONTRIBUTIONS

Conceptualization, W.S., D.E.I., and H.J.K.; Methodology, W.S. and H.J.K.; Investigation, W.S., C.D.H., D.E.I., and H.J.K.; Writing, W.S., D.E.I., and H.J.K.; Funding Acquisition, D.E.I. and H.J.K.; Supervision, H.J.K.

DECLARATION OF INTERESTS

H.J.K. is a founder of 3D Health Solutions Inc. and holds an equity interest in the company. D.E.I. is a founder of Emulate Inc. and chairs its Scientific Advisory Board. D.E.I. and C.D.H. also hold equity in the company. D.E.I., C.D.H., and H.J.K. are listed as inventors on multiple related patents.

Received: August 20, 2018
Revised: December 28, 2018
Accepted: April 29, 2019
Published: May 31, 2019

REFERENCES

Aguilera, O., and Munoz, A. (2007). DKK1 (dickkopf homolog 1 (*Xenopus laevis*)). Atlas Genet. Cytogenet. Oncol. Haematol. *11*, 266–267.

Bafico, A., Gazit, A., Pramila, T., Finch, P.W., Yaniv, A., and Aaronson, S.A. (1999). Interaction of frizzled related protein (FRP) with Wnt ligands and the frizzled receptor suggests alternative mechanisms for FRP inhibition of Wnt signaling. J. Biol. Chem. *274*, 16180–16187.

Bafico, A., Liu, G., Yaniv, A., Gazit, A., and Aaronson, S.A. (2001). Novel mechanism of Wnt signalling inhibition mediated by Dickkopf-1 interaction with LRP6/Arrow. Nat. Cell. Biol. *3*, 683–686.

Biswas, S., Davis, H., Irshad, S., Sandberg, T., Worthley, D., and Leedham, S. (2015). Microenvironmental control of stem cell fate in intestinal homeostasis and disease. J. Pathol. *237*, 135–145.

Bovolenta, P., Esteve, P., Ruiz, J.M., Cisneros, E., and Lopez-Rios, J. (2008). Beyond Wnt inhibition: new functions of secreted Frizzled-related proteins in development and disease. J. Cell Sci. *121*, 737–746.

Clevers, H., Loh, K.M., and Nusse, R. (2014). Stem cell signaling. An integral program for tissue renewal and regeneration: Wnt signaling and stem cell control. Science *346*, 1248012.

Crosnier, C., Stamataki, D., and Lewis, J. (2006). Organizing cell renewal in the intestine: stem cells, signals and combinatorial control. Nat. Rev. Genet. *7*, 349–359.

De Bosscher, K., and Nicolas, F.J. (2004). Molecular and functional consequences of Smad4 C-terminal missense mutations in colorectal tumour cells. Biochem. J. *379*, 209–216.

Du, Q., Zhang, X., Liu, Q., Zhang, X., Bartels, C.E., and Geller, D.A. (2013). Nitric oxide production upregulates Wnt/beta-catenin signaling by inhibiting Dickkopf-1. Cancer Res. *73*, 6526–6537.

Ettayebi, K., Crawford, S.E., Murakami, K., Broughman, J.R., Karandikar, U., Tenge, V.R., Neill, F.H., Blutt, S.E., Zeng, X.-L., Qu, L., et al. (2016). Replication of human noroviruses in stem cell–derived human enteroids. Science *353*, 1387–1393.

Farin, H.F., Jordens, I., Mosa, M.H., Basak, O., Korving, J., Tauriello, D.V., de Punder, K., Angers, S., Peters, P.J., and Maurice, M.M. (2016). Visualization of a short-range Wnt gradient in the intestinal stem-cell niche. Nature *530*, 340–343.

Farin, H.F., Van Es, J.H., and Clevers, H. (2012). Redundant sources of Wnt regulate intestinal stem cells and promote formation of Paneth cells. Gastroenterology *143*, 1518–1529.e7.

Fung, K.Y., Fairn, G.D., and Lee, W.L. (2018). Transcellular vesicular transport in epithelial and endothelial cells: Challenges and opportunities. Traffic *19*, 5–18.

Gao, D., Liu, H., Lin, J.M., Wang, Y., and Jiang, Y. (2013). Characterization of drug permeability in Caco-2 monolayers by mass spectrometry on a membrane-based microfluidic device. Lab Chip *13*, 978–985.

Gavin, B.J., McMahon, J.A., and McMahon, A.P. (1990). Expression of multiple novel Wnt-1/int-1-related genes during fetal and adult mouse development. Genes Dev. *4*, 2319–2332.

Glinka, A., Wu, W., Delius, H., and Monaghan, A.P. (1998). Dickkopf-1 is a member of a new family of secreted proteins and functions in head induction. Nature *391*, 357–362.

Gonzalez-Sancho, J.M., Aguilera, O., Garcia, J.M., Pendas-Franco, N., Pena, C., Cal, S., Garcia de Herreros, A., Bonilla, F., and Munoz, A. (2005). The Wnt antagonist DICKKOPF-1 gene is a downstream target of beta-catenin/TCF and is downregulated in human colon cancer. Oncogene *24*, 1098–1103.

Granger, D. (1981). Intestinal microcirculation and transmucosal fluid transport. Am. J. Physiol. Gastrointest. Liver Physiol. *240*, G343–G349.

Huh, D., Kim, H.J., Fraser, J.P., Shea, D.E., Khan, M., Bahinski, A., Hamilton, G.A., and Ingber, D.E. (2013). Microfabrication of human organs-on-chips. Nat. Protoc. *8*, 2135–2157.

Ilyas, M., Tomlinson, I.P., Rowan, A., Pignatelli, M., and Bodmer, W.F. (1997). Beta-catenin mutations in cell lines established from human colorectal cancers. Proc. Natl. Acad. Sci. U S A *94*, 10330–10334.

Imura, Y., Asano, Y., Sato, K., and Yoshimura, E. (2009). A microfluidic system to evaluate intestinal absorption. Anal. Sci. *25*, 1403–1407.

Johnson, F.P. (1910). The development of the mucous membrane of the oesophagus, stomach, and small intestine in the human embryo. Am. J. Anat. *10*, 521–561.

Kammeraad, A. (1942). The development of the gastrointestinal tract of the rat. I. Histogenesis of the epithelium of the stomach, small intestine and pancreas. J. Morphol. *70*, 323–342.

Kasendra, M., Tovaglieri, A., Sontheimer-Phelps, A., Jalili-Firoozinezhad, S., Bein, A., Chalkiadaki, A., Scholl, W., Zhang, C., Rickner, H., and Richmond, C.A. (2018). Development of a primary human Small Intestine-on-a-Chip using biopsy-derived organoids. Sci. Rep. *8*, 2871.

Kawano, Y., and Kypta, R. (2003). Secreted antagonists of the Wnt signalling pathway. J. Cell Sci. *116*, 2627–2634.

Kim, H.J., Huh, D., Hamilton, G., and Ingber, D.E. (2012). Human gut-on-a-chip inhabited by microbial flora that experiences intestinal peristalsis-like motions and flow. Lab Chip *12*, 2165–2174.

Kim, H.J., and Ingber, D.E. (2013). Gut-on-a-Chip microenvironment induces human intestinal cells to undergo villus differentiation. Integr. Biol. *5*, 1130–1140.

Kim, H.J., Li, H., Collins, J.J., and Ingber, D.E. (2016). Contributions of microbiome and mechanical deformation to intestinal bacterial overgrowth and inflammation in a human gut-on-a-chip. Proc. Natl. Acad. Sci. U S A *113*, E7–E15.

Koch, S., Capaldo, C.T., Samarin, S., Nava, P., Neumaier, I., Skerra, A., Sacks, D.B., Parkos, C.A., and Nusrat, A. (2009). Dkk-1 inhibits intestinal epithelial cell migration by attenuating directional polarization of leading edge cells. Mol. Biol. Cell *20*, 4816–4825.

Kuhnert, F., Davis, C.R., Wang, H.T., Chu, P., Lee, M., Yuan, J., Nusse, R., and Kuo, C.J. (2004). Essential requirement for Wnt signaling in proliferation of adult small intestine and colon revealed by adenoviral expression of Dickkopf-1. Proc. Natl. Acad. Sci. U S A *101*, 266–271.

Logan, C.Y., and Nusse, R. (2004). The Wnt signaling pathway in development and disease. Annu. Rev. Cell Dev. Biol. *20*, 781–810.

Malinauskas, T., Aricescu, A.R., Lu, W., Siebold, C., and Jones, E.Y. (2011). Modular mechanism of Wnt signaling inhibition by Wnt inhibitory factor 1. Nat. Struct. Mol. Biol. *18*, 886–893.

Martini, E., Krug, S.M., Siegmund, B., Neurath, M.F., and Becker, C. (2017). Mend your fences: the epithelial barrier and its relationship with mucosal immunity in inflammatory bowel disease. Cell. Mol. Gastroenterol. Hepatol. *4*, 33–46.

Mehta, D., and Malik, A.B. (2006). Signaling mechanisms regulating endothelial permeability. Physiol. Rev. *86*, 279–367.

Munemitsu, S., Albert, I., Souza, B., Rubinfeld, B., and Polakis, P. (1995). Regulation of intracellular beta-catenin levels by the adenomatous polyposis coli (APC) tumor-suppressor protein. Proc. Natl. Acad. Sci. U S A *92*, 3046–3050.

Noel, G., Baetz, N.W., Staab, J.F., Donowitz, M., Kovbasnjuk, O., Pasetti, M.F., and Zachos, N.C. (2017). A primary human macrophage-enteroid co-culture model to investigate mucosal gut physiology and host-pathogen interactions. Sci. Rep. *7*, 45270.

Ootani, A., Li, X., Sangiorgi, E., Ho, Q.T., Ueno, H., Toda, S., Sugihara, H., Fujimoto, K., Weissman, I.L., Capecchi, M.R., et al. (2009). Sustained in vitro intestinal epithelial culture within a Wnt-dependent stem cell niche. Nat. Med. *15*, 701–706.

Peifer, M., and Polakis, P. (2000). Wnt signaling in oncogenesis and embryogenesis–a look outside the nucleus. Science *287*, 1606–1609.

Petersen, C.P., and Reddien, P.W. (2009). Wnt signaling and the polarity of the primary body axis. Cell *139*, 1056–1068.

Pinto, D., Gregorieff, A., Begthel, H., and Clevers, H. (2003). Canonical Wnt signals are essential for homeostasis of the intestinal epithelium. Genes Dev. *17*, 1709–1713.

Powell, D., Pinchuk, I., Saada, J., Chen, X., and Mifflin, R. (2011). Mesenchymal cells of the intestinal lamina propria. Annu. Rev. Physiol. *73*, 213–237.

Pusch, J., Votteler, M., Gohler, S., Engl, J., Hampel, M., Walles, H., and Schenke-Layland, K. (2011). The physiological performance of a three-dimensional model that mimics the microenvironment of the small intestine. Biomaterials *32*, 7469–7478.

Ramond, M.J., Martinot-Peignoux, M., and Erlinger, S. (1985). Dome formation in the human colon carcinoma cell line Caco-2 in culture. Influence of ouabain and permeable supports. Biol. Cell *54*, 89–92.

Roulis, M., and Flavell, R.A. (2016). Fibroblasts and myofibroblasts of the intestinal lamina propria in physiology and disease. Differentiation *92*, 116–131.

Saaf, A.M., Halbleib, J.M., Chen, X., Yuen, S.T., Leung, S.Y., Nelson, W.J., and Brown, P.O. (2007). Parallels between global transcriptional programs of polarizing Caco-2 intestinal epithelial cells in vitro and gene expression programs in normal colon and colon cancer. Mol. Biol. Cell *18*, 4245–4260.

Sato, T., and Clevers, H. (2013). Growing self-organizing mini-guts from a single intestinal stem cell: mechanism and applications. Science *340*, 1190–1194.

Sato, T., van Es, J.H., Snippert, H.J., Stange, D.E., Vries, R.G., van den Born, M., Barker, N., Shroyer, N.F., van de Wetering, M., and Clevers, H. (2011). Paneth cells constitute the niche for Lgr5 stem cells in intestinal crypts. Nature *469*, 415–418.

Sato, T., Vries, R.G., Snippert, H.J., van de Wetering, M., Barker, N., Stange, D.E., van Es, J.H., Abo, A., Kujala, P., Peters, P.J., et al. (2009). Single Lgr5 stem cells build crypt-villus structures in vitro without a mesenchymal niche. Nature *459*, 262–265.

Saxena, K., Blutt, S.E., Ettayebi, K., Zeng, X.-L., Broughman, J.R., Crawford, S.E., Karandikar, U., Sastri, N.P., Conner, M.E., and Opekun, A. (2015). Human intestinal enteroids: a new model to study human rotavirus infection, host restriction and pathophysiology. J. Virol. *90*, 43–56.

Scoville, D.H., Sato, T., He, X.C., and Li, L. (2008). Current view: intestinal stem cells and signaling. Gastroenterology *134*, 849–864.

Shin, W., and Kim, H.J. (2018). Intestinal barrier dysfunction orchestrates the onset of inflammatory host–microbiome cross-talk in a human gut inflammation-on-a-chip. Proc. Natl. Acad. Sci. U S A *115*, E10539–E10547.

Shin, W., Wu, A., Massidda, M.W., Foster, C., Thomas, N., Lee, D.-W., Koh, H., Ju, Y., Kim, J., and Kim, H.J. (2019). A robust longitudinal co-culture of obligate anaerobic gut microbiome with human intestinal epithelium in an anoxic-oxic interface-on-a-chip. Front. Bioeng. Biotechnol. *7*, 13.

Sick, S., Reinker, S., Timmer, J., and Schlake, T. (2006). WNT and DKK determine hair follicle spacing through a reaction-diffusion mechanism. Science *314*, 1447–1450.

Spence, J.R., Lauf, R., and Shroyer, N.F. (2011). Vertebrate intestinal endoderm development. Dev. Dyn. *240*, 501–520.

Takahashi, N., Fukushima, T., Yorita, K., Tanaka, H., Chijiiwa, K., and Kataoka, H. (2010). Dickkopf-1 is overexpressed in human pancreatic ductal adenocarcinoma cells and is involved in invasive growth. Int. J. Cancer *126*, 1611–1620.

Valenta, T., Degirmenci, B., Moor, A.E., Herr, P., Zimmerli, D., Moor, M.B., Hausmann, G., Cantu, C., Aguet, M., and Basler, K. (2016). Wnt ligands secreted by subepithelial mesenchymal cells are essential for the survival of intestinal stem cells and gut homeostasis. Cell Rep. *15*, 911–918.

Voloshanenko, O., Erdmann, G., Dubash, T.D., Augustin, I., Metzig, M., Moffa, G., Hundsrucker, C., Kerr, G., Sandmann, T., Anchang, B., et al. (2013). Wnt secretion is required to maintain high levels of Wnt activity in colon cancer cells. Nat. Commun. *4*, 2610.

Walton, K.D., Kolterud, A., Czerwinski, M.J., Bell, M.J., Prakash, A., Kushwaha, J., Grosse, A.S., Schnell, S., and Gumucio, D.L. (2012). Hedgehog-responsive mesenchymal clusters direct patterning and emergence of intestinal villi. Proc. Natl. Acad. Sci. U S A *109*, 15817–15822.

Yan, Q., Wu, X., Chen, C., Diao, R., Lai, Y., Huang, J., Chen, J., Yu, Z., Gui, Y., and Tang, A. (2012). Developmental expression and function of DKKL1/Dkkl1 in humans and mice. Reprod. Biol. Endocrinol. *10*, 51.

Zallen, J.A. (2007). Planar polarity and tissue morphogenesis. Cell *129*, 1051–1063.

ISCI, Volume *15*

Supplemental Information

Human Intestinal Morphogenesis Controlled by Transepithelial Morphogen Gradient and Flow-Dependent Physical Cues in a Microengineered Gut-on-a-Chip

Woojung Shin, Christopher D. Hinojosa, Donald E. Ingber, and Hyun Jung Kim

SUPPLEMENTAL INFORMATION

SUPPLEMENTAL FIGURES

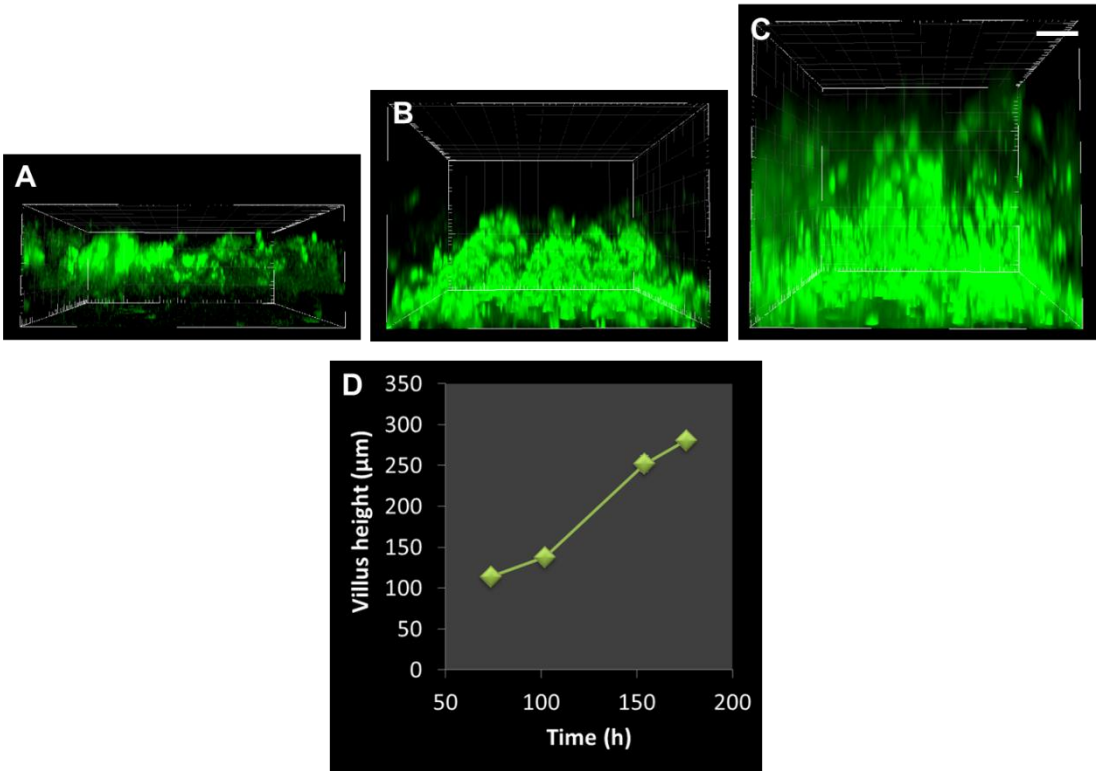

Figure S1. Growth profile of Caco-2 villi-like epithelium in the Gut Chip. Related to Figure 1. (A-C) The 3D rendered morphology of Caco-2 villi-like structure that were grown in the Gut Chip with a height of the upper microchannel at 500 µm. Z-stacked images were taken at 74 (A), 102 (B) and 176 hr (C). Live cell imaging was performed after flowing Calcein AM (5 µM, final concentration) for 30 min by confocal microscopy. (D) Quantification of the villi-like epithelial height as a function of time (S.E.M.; The sizes of error bars are smaller than the symbol). Bar, 50 µm.

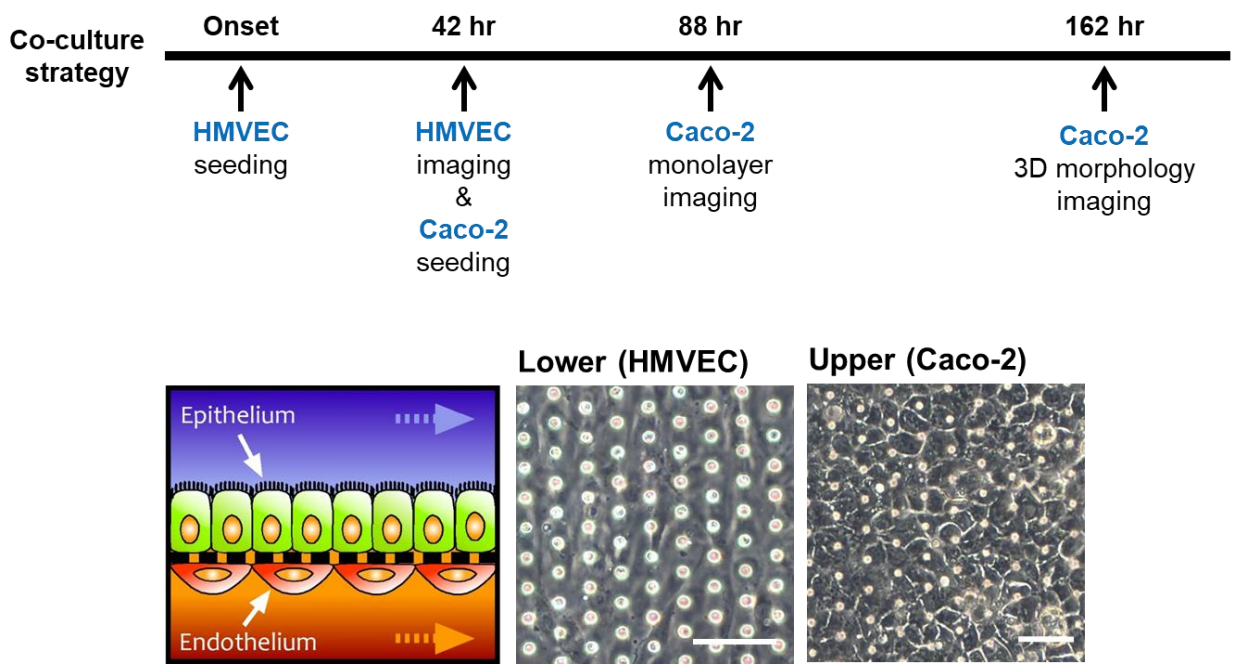

Figure S2. Morphology of Caco-2 and human microvascular endothelial cells (HMVEC) lined on one and the opposite side of the porous membrane in a Gut Chip. Related to Figure 1. The experimental procedure of co-cultures (top). The lower panel shows a schematic of experimental design (left) and phase contrast images of HMVEC (middle) and Caco-2 (right) monolayers. A HMVEC monolayer pre-formed on the porous membrane in the lower microchannel prevented basolateral shear stress to the Caco-2 cells. Bars, 50 μm.

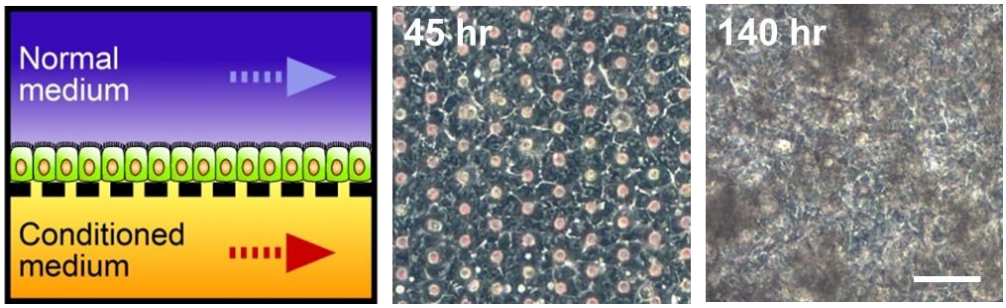

Figure S3. The basolateral flow of the conditioned medium that is collected from the Caco-2 cells suppresses the villi-like epithelial growth in the Gut Chip. Related to Figure 2. The conditioned medium was collected from the basolateral side of a Caco-2 monolayer grown in a Transwell porous insert. An experimental setup (left). Phase contrast images were taken at 45 (middle) and 140 hr (right), respectively. The conditioned medium was applied in the lower microchannel at 20 hr after a cell monolayer was achieved in the Gut Chip. Bar, 50 μm.

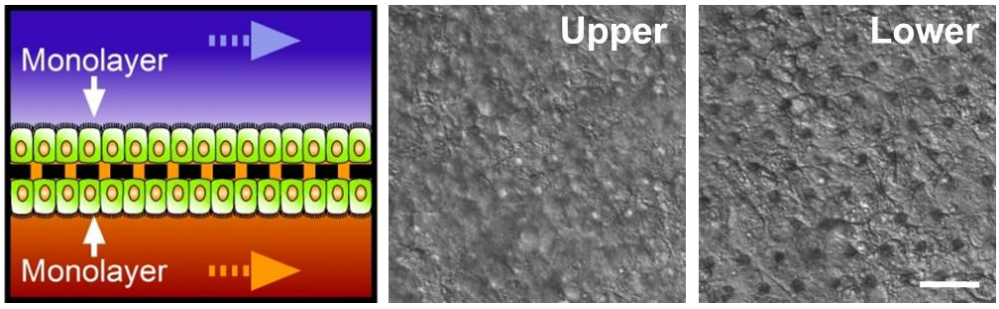

Figure S4. Bi-layered Caco-2 cells grown in a Gut Chip prevent the formation of villi-like structure. Related to Figure 2. An experimental setup (left). Caco-2 cells failed to form villi-like structure when they were simultaneously grown on the same porous membrane in the lumen (upper) and capillary (lower) microchannels. DIC microscopic views were recorded to visualize the monolayers established on each microchannel at 150 hr. Bar, 50 μm.

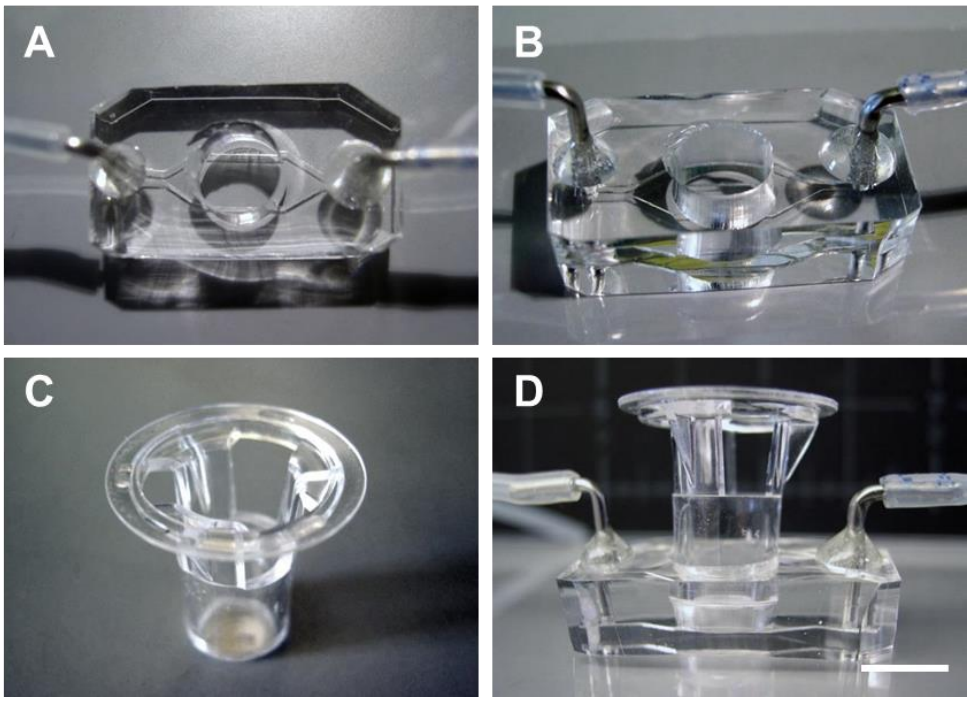

Figure S5. A Transwell-insertable hybrid microfluidic device. Related to Figure 2. (A) A top-down view and (B) an angled view of a hybrid device that contains an upper layer with a circular Transwell-insertable hole and two connecting ports as an inlet and an outlet to supply fresh culture medium into the basolateral side of a Transwell. A lower microchannel (height, 200 μm) directly contacts to the basolateral side of a Transwell insert. (C) A 24 well-fit Transwell insert (surface area, 0.33 cm^2). (D) A side view of the hybrid device holding a Transwell insert. Bar, 1 cm.

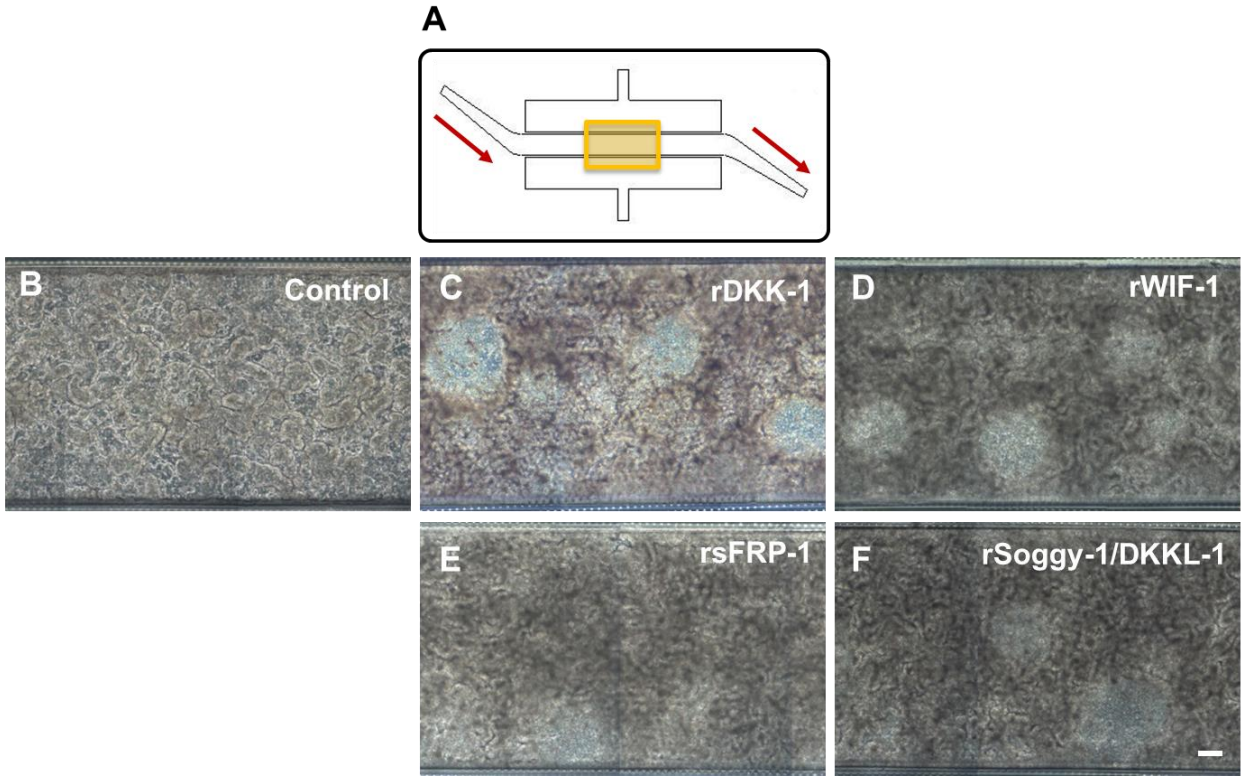

Figure S6. Loss of villi-like structure after treatment of various Wnt antagonists. Related to Figure 4. (A) A top-down schematic of a Gut Chip. A yellow box in the schematic shows the location of the phase contrast image in each experimental setup. Arrows indicate the flow direction of the medium. (B-F) Villus-like morphologies in the Gut Chip in the absence (B, Control) or the presence of recombinant Wnt antagonists (C, rDKK-1; D, rWIF-1; E, rsFRP-1; and F, rSoggy-1/DKKL-1). Wnt antagonists were flowed into the lower microchannel for 48 hr, then the setup was imaged by phase contrast microscopy. Bar, 100 μm.

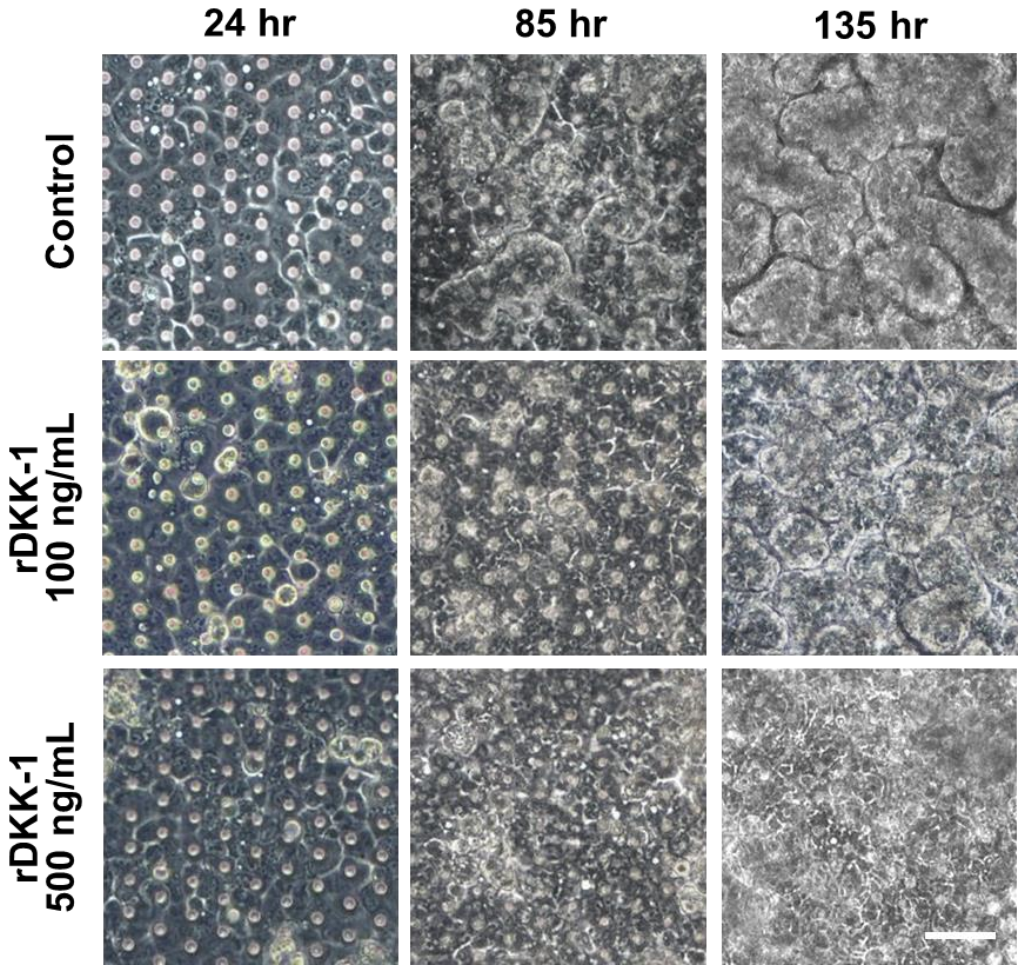

Figure S7. rDKK-1 inhibits the 3D epithelial growth of Caco-2 cells in a dose-dependent manner. Related to Figure 4. A time course of the epithelial growth at different concentrations of rDKK-1 (100 and 500 ng/mL; Control at 0 ng/mL). The culture medium containing rDKK-1 was perfused into the basolateral microchannel at 72 hr since the seeding. Phase contrast images were taken at 24, 85, and 135 hr, respectively. The image taken at 135 hr was also provided in Figure 4C. Bar, 50 μm.

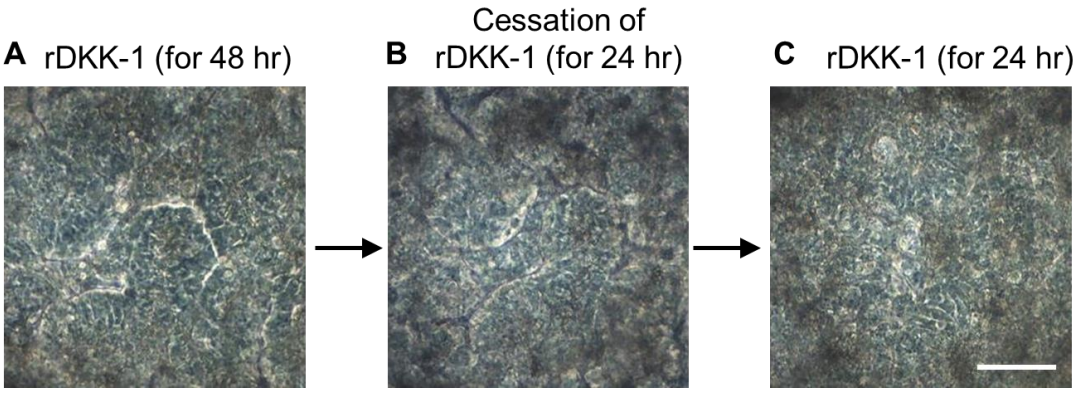

Figure S8. Regeneration of villi-like epithelium in response to the treatment and cessation of rDKK-1. Related to Figure 4. (A) Treatment of rDKK-1 (500 ng/mL) to the pre-grown villi-like epithelium for 48 hr induced the loss of villi-like structure. A fixed position where the epithelial destruction is distinctly shown in “A” was periodically monitored by the phase contrast microscopy. (B) Cessation of rDKK-1 treatment induced the regeneration of villi-like structure within 24 hr. (C) Retreatment of rDKK-1 induced epithelial disruption within 24 hr. Bar, 50 μm.

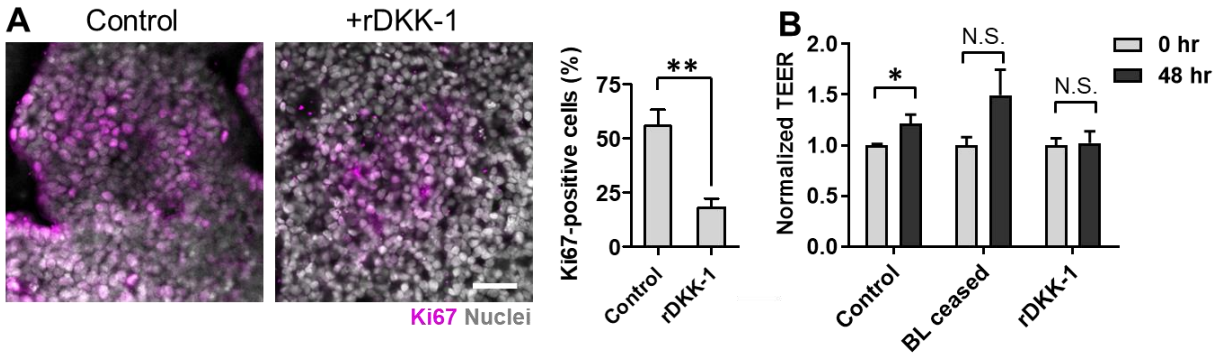

Figure S9. The decreased population of proliferative cells in response to rDKK-1 treatment. Related to Figure 4. (A) Treatment of rDKK-1 (500 ng/mL) to the pre-grown 3D intestinal epithelium in a Gut Chip for 48 hr resulted in a reduced population of Ki67-positive proliferative cells (N=5). Overlaid images taken by the confocal microscopy visualizes the Ki67-positive cells (magenta) and the nuclei of total cells (grey). The number of Ki67-positive cells as well as the total cells were manually counted and quantitated (a chart). (B) Barrier function, assessed by measuring transepithelial electrical resistance (TEER), after the treatment of rDKK-1 or cessation of basolateral flow for 48 hr was maintained without statistical significance (N=10). Bar, 50 μm. N.S., not significant. *p<0.05, **p<0.001.

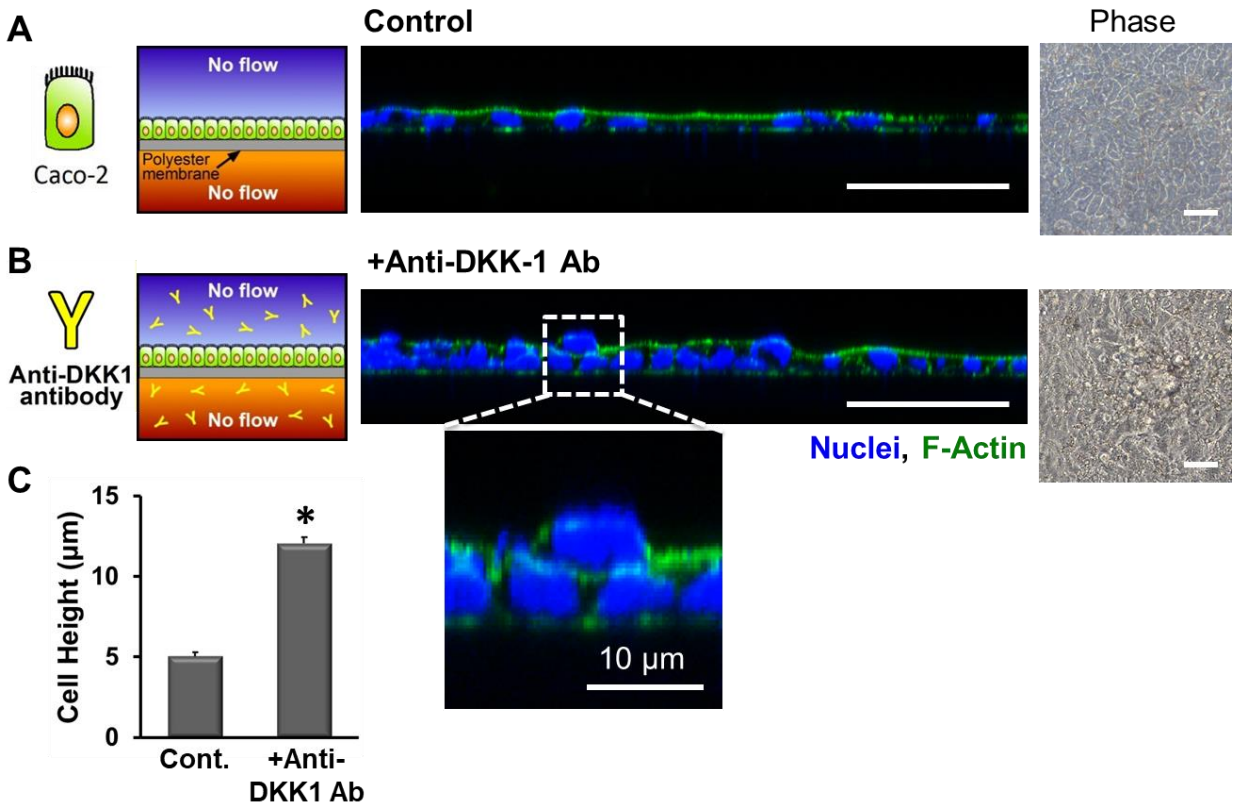

Figure S10. Initiation of villi-like growth in the presence of anti-DKK-1 antibodies in the Caco-2 monolayer grown on a Transwell. Related to Figure 4. (A-B) Schematics (left), cross-cut views of the fluorescently labeled monolayers with nuclei (blue) and F-actin (green) (middle), and phase contrast images (right) of the Caco-2 cells. (A) The Control (without anti-DKK-1 Ab) shows a flat monolayer with a planar morphology (cell height, 5.05±0.25 μm). (B) Addition of anti-DKK-1 Ab ("Anti-DKK-1 Ab"; 20 μg/mL) for 72 hr to both apical and basolateral sides in the Transwell induces increased cell height (12.07±0.36 μm) with statistical significance (*p<0.0001). Confocal microscopy visualizes. A zoomed-in inset shows the superposition of a cell above the monolayer, suggesting the initiation of morphogenesis. A phase contrast image visualizes the villi-like undulation. (C) Quantification of the height of monolayers. 'Cont.' means Control. N=20. Bars, 30 μm.

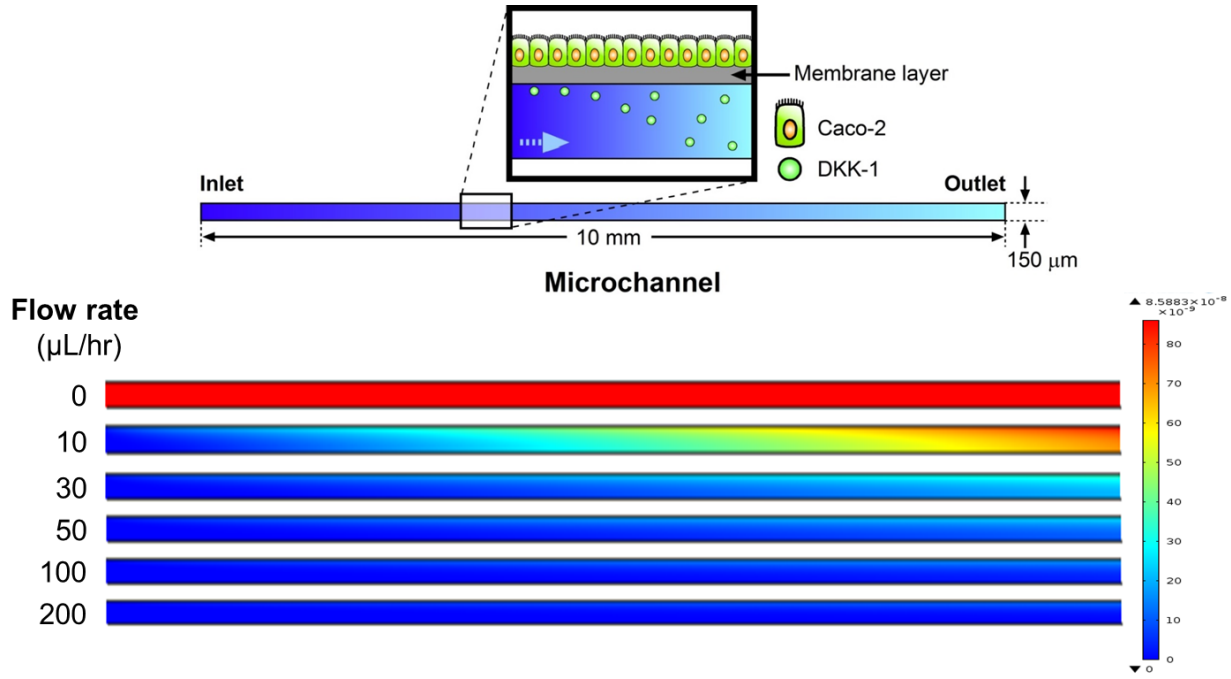

Figure S11. The 2D computational simulation of the basolateral secretion and subsequent diffusion of DKK-1 molecules in a Gut Chip at various flow rates. Related to Figure 5. A schematic (top) shows the 2D side view of a lower microchannel (Blue inlet, sky blue outlet), and the zoom-in inset configures the secretion of DKK-1 from the basal surface of a Caco-2 monolayer into the capillary microchannel. In the flow rate regime from 0 to 200 μL/hr, 2D simulations were performed at conditions as the DKK-1 production rate by Caco-2 cells is 42.1 pg/10^5 cells/hr (Koch et al., 2009), number of cells was 5×10^5 cells, and the diffusion coefficient of DKK-1 was 1×10^{-10} cm^2/sec (Sick et al., 2006). Pores and their structure in the PDMS membrane were simplified by adding a diffusion layer ("Membrane layer" in the zoom-in inset) during simulation where no fluid advection took place. A color bar (bottom right) indicates the scaled range of DKK-1 concentrations (unit, mol/m^3).

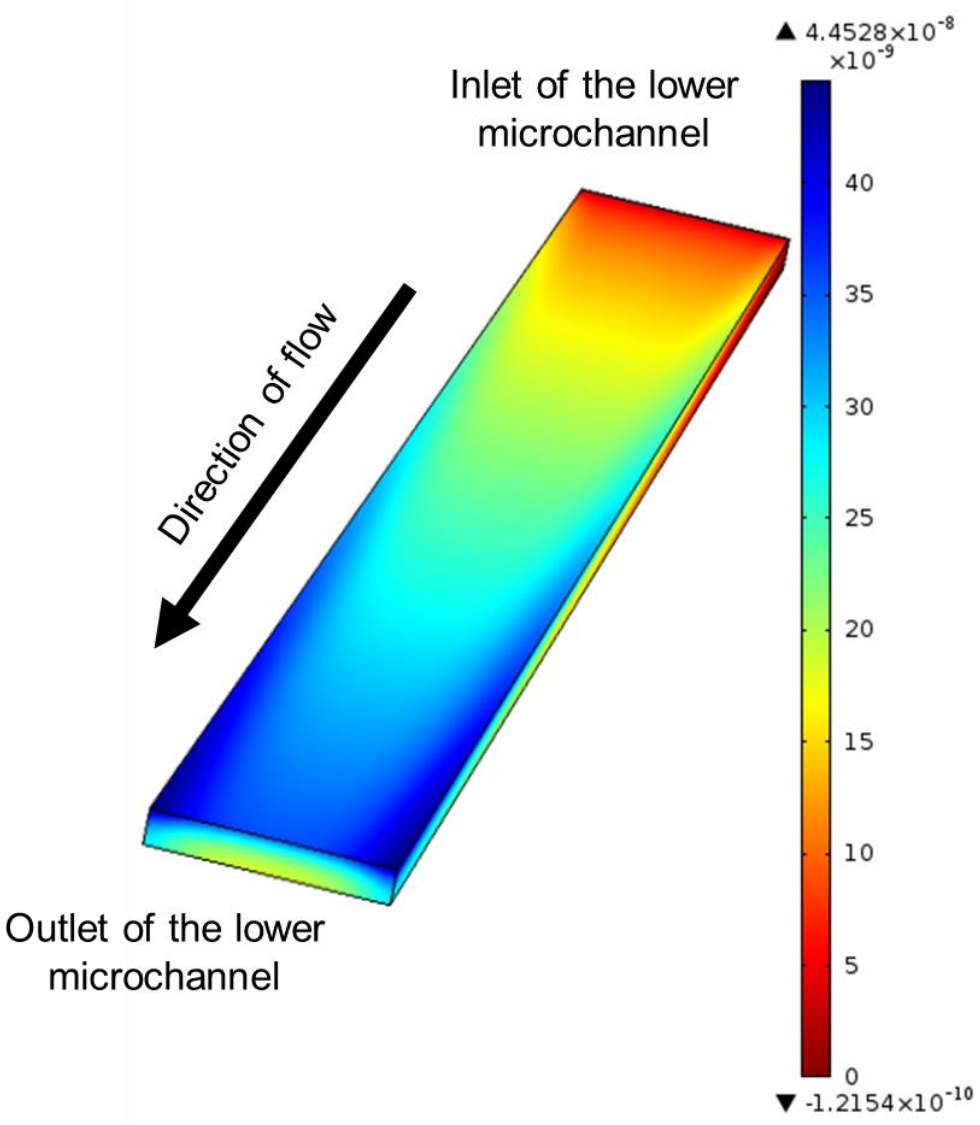

Figure S12. The concentration profile of DKK-1 in the basal microchannel of a Gut Chip. Related to Figure 5. The 3D volume represents the geometry of the lower microchannel. A heat map shows the concentration profile of DKK-1 in the capillary microchannel. The upper plane of this 3D heat map represents the basolateral space underneath the porous membrane that touches the basal membrane of a Caco-2 epithelium in the upper microchannel. The concentration of DKK-1 near the inlet of the microchannel was relatively low whereas its level increased by 10-fold or more in regions near the channel outlet. A 2D top-view of this heat map was used in Figure 5A. A color bar (right) indicates the scaled range of DKK-1 concentrations (unit, mol/m^3).

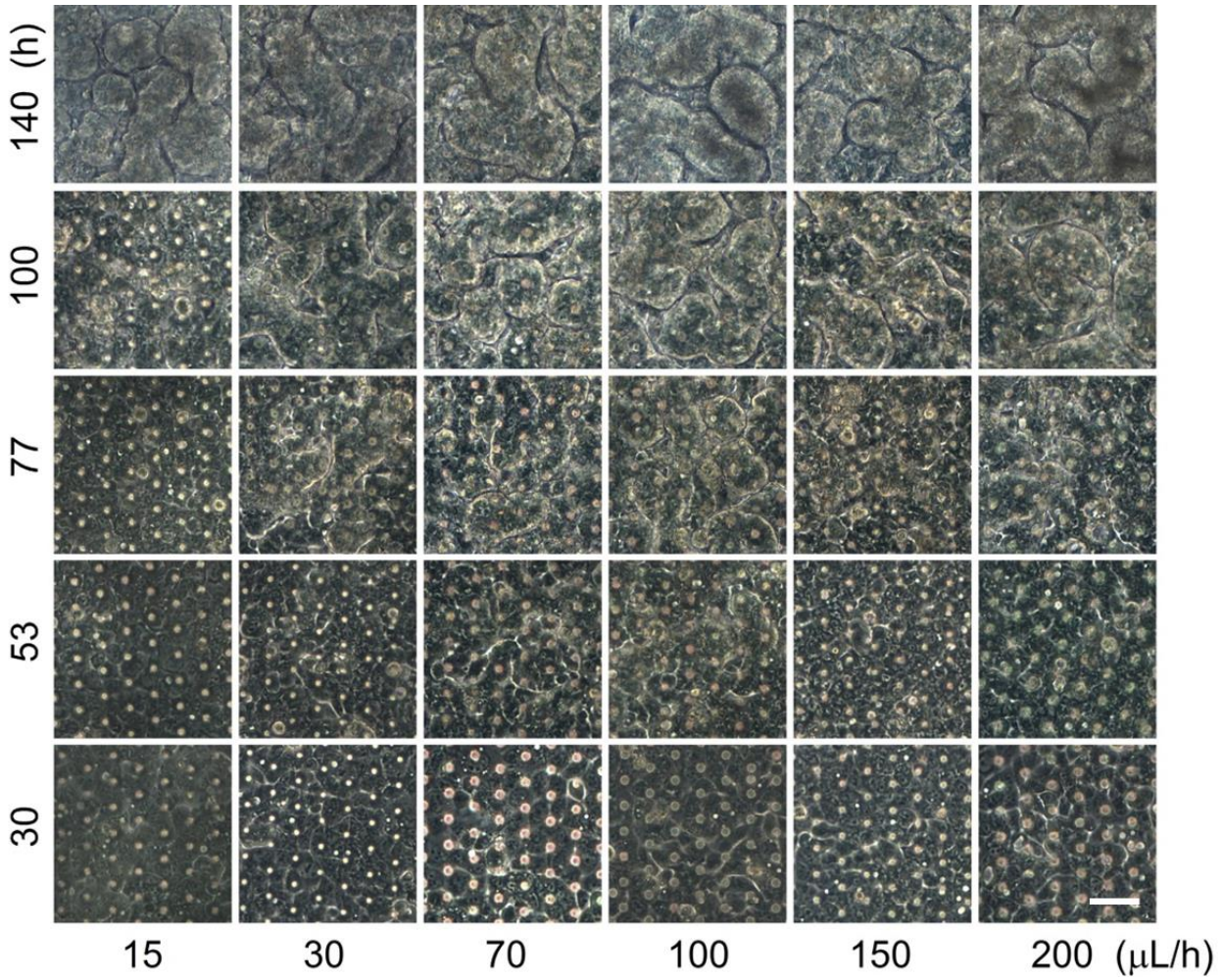

Figure S13. Temporal profile of the villi-like morphogenesis of Caco-2 cells in a Gut Chip as a function of flow rates. Related to Figure 6. Phase contrast microscopy was applied to take snapshots of villi at 30, 53, 77, 100, and 140 hr, respectively. Volumetric flow rates were applied at 15, 30, 70, 100, 150, and 200 μL/hr, respectively. Results of epithelial height were plotted in Figure 6A. Bar, 50 μm.

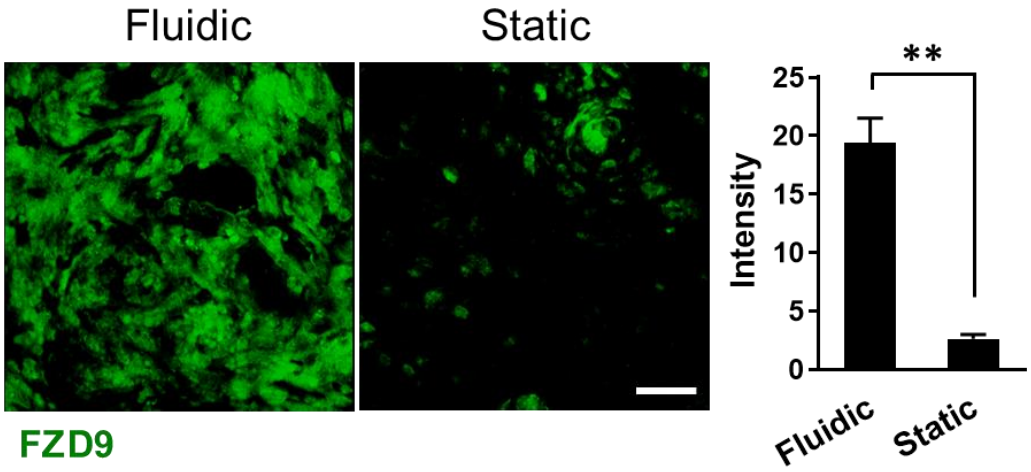

Figure S14. FZD9 expression of the human organoid-derived epithelium cultured in a hybrid microfluidic chip. Related to Figure 6. Human colonoid-derived epithelial cells were cultured in the hybrid chip with ("Fluidic") or without ("Static") basolateral flow for 168 hr, and the expression of FZD9 was analyzed by immunofluorescence imaging. Images represent the projection view of the 3D reconstructed images. The intensity of FZD9 was quantified using Image J (N=3). Bar, 50 μm. ** $p<0.001$.

TRANSPARENT METHODS

Microfabrication of a Device. A Gut Chip microdevice was fabricated by the soft lithography method as previously described (Kim et al., 2012). Briefly, a Gut Chip was fabricated with the upper and lower microchannel compartments of cured polydimethylsiloxane (PDMS, 15:1 (w/w) prepolymer:curing agent; Sylgard, Dow Corning). A Gut Chip has two parallel cell culture microchannels (1 mm wide × 10 mm long × 0.15 mm high) and two vacuum chambers (1.68 mm × 9.09 mm × 0.15 mm) besides the central cell channels. Each microchannel is separated by a PDMS wall (100 μm thick). A porous PDMS membrane (20 μm thick) containing an array of circular pores (10 μm diameter with 25 μm spacing) was produced as described (Kim et al., 2012). The layer-by-layer assembly of each PDMS compartment and a porous membrane was performed by incubating the setup at 80°C for an overnight after corona treatment (BD-20AC, Electro-Technic Products, Inc.). Gas-permeable silicone tubing (Tygon 3350, ID 1/32", OD 3/32", Saint-Gobain Performance Plastics) linked with a connector (hub-free stainless steel blunt needle, 18G; Kimble Chase) was inserted into the microchannels to supply cell culture medium (Figure 1A, orange and blue arrows) or vacuum suction (Figure 1A, white arrows). To test the effect of apical shear stress on the epithelial morphogenesis (Figure 1F), a single channel microfluidic device was prepared by bonding the upper PDMS layer of a Gut Chip onto a flat PDMS layer via corona treatment bonding as previously described. To monitor the maximum epithelial growth (Figure S1), we used an upper microfluidic layer with the same design of a Gut Chip but the modified height from 0.2 to 1 mm. A Transwell-insertable hybrid microfluidic device (Figures 2B middle, 2C left, and S5) that can hold a Transwell insert (pore size, 0.45 μm; culture area, 0.33 cm^2) was fabricated by bonding the Transwell-insertable upper and the microfluidic lower (150 μm in height) layers through corona treatment.

Cell Culture. A Caco-2BBE human intestinal epithelial cell line was purchased from the Harvard Digestive Disease Center. Conventional static cultures of Caco-2 cells were performed in a Transwell (pore size of a polyester membrane, 0.45 μm; culture area, 0.33 cm^2). The complete culture medium includes 20% (v/v) fetal bovine serum (FBS; Gibco), 100 units/mL penicillin, and 100 μg/mL streptomycin (Gibco) in the Dulbecco's Modified Eagle Medium (DMEM; Gibco) containing 4.5 g/L glucose and 25 mM HEPES. Complete medium was replenished every other day in both apical (AP) and basolateral (BL) sides until use. To prepare a conditioned medium (Figure S3), we cultured Caco-2 cells in the Transwell (N=20), then collected the conditioned medium from the BL side at day 3 since the seeding. The collected conditioned medium was spun down (500× *g*, 5 min) to remove possible cell debris; then the supernatant was used. To carry out Transwell perfusion test (Figure 2B, middle and 2C, left) or diffusion test (Figure 2B, right), we used 3-week-cultured Caco-2 cells, or 1-week-cultured human intestinal organoid cells on Transwell inserts. For the diffusion test (Figure 2B, right), a Transwell insert containing a pre-cultured Caco-2 monolayer was placed in the center of a 6" tissue culture dish (Corning) using two rectangular PDMS spacers (0.5 cm wide × 1 cm long × 1 cm high), then added 70 mL (100-fold increased volume from the format in a 24-well plate) of the complete culture medium into the BL side. Incubation was further performed for 120 hr from the onset in the 6" dish culture.

Organoid Culture. Human primary intestinal organoids derived from colonic biopsy (C103; ascending colon) of a healthy donor (Rajan et al., 2018) were cultured embedded in Matrigel (BD Biosciences) with 500 µL of the organoid complete medium in a 24 well plate, then incubated in a humidified CO_2 incubator at 37°C. Organoid complete medium was composed of a basal medium that contains 10 mM HEPES (Gibco), 1× GlutaMAX (Invitrogen), 100 units/mL penicillin, and 100 µg/mL streptomycin in Advanced DMEM/F-12 (Gibco) and conditioned medium of Wnt3A, R-spondin, and noggin, in which the volume ratio of basal and each conditioned medium is defined at 20/50/20/10% (v/v). In the mixture of basal and conditioned medium, murine recombinant EGF (50 ng/mL; Peprotech), SB202190 (30 µM; Sigma Aldrich), A-8301 (500 nM; Sigma Aldrich), Gastrin (10 nM; Sigma Aldrich), *N*-acetylcysteine (1 mM; MP Biomedicals), nicotinamide (10 mM; Sigma Aldrich), N2 (1×; Gibco), and B27 (1×; Gibco) were added. Conditioned medium was prepared by culturing Wnt-3A-producing L cells (ATCC, CRL 2647), Rspo1 cells (Trevigen), and Noggin secreting cells (Baylor's College of Medicine) based on the literature (Sato et al., 2011; Saxena et al., 2015). Organoid complete medium was changed every other day, and organoids were passed once a week by mechanically breaking down the organoids, spinning down the fragmented organoids (100× *g*, 4°C, 5 min), resuspending centrifuged organoids with fresh Matrigel on ice, then plating them in each well of a 24 well plate.

For the Transwell culture of human intestinal organoid-derived primary epithelial cells, 3D colonoids were dissociated into single cells by applying 500 µL of EDTA solution (0.5 mM; Alfa Aesar), breaking the Matrigel, collecting organoid pellets after centrifugation (100× *g*, 4°C, 5 min), and incubating with 1 mL of TrypLE (Gibco) at 37°C for 15 min. After filtering the cell suspension through a cell strainer (40 µm pores, Corning), dissociated organoid epithelial cells resuspended in organoid complete medium (final cell density, ~6×10^6 cells/mL) were seeded into a Transwell insert. A monolayer of colonoid-derived epithelium was formed by replacing the culture medium every other day for up to a week.

Microfluidic Cell Cultures. Prior to seeding Caco-2 or normal colonoid-derived epithelial cells, a Gut Chip was sterilized by flowing 70% (v/v) ethanol into the microchannels, completely dried in an 80°C oven, then exposed to ultraviolet light and ozone simultaneously (UVO Cleaner 342, Jelight Company Inc.) for either 40 min (for Caco-2 cells) or 1 hr (for organoid-derived epithelial cells). After microchannels were coated with a mixture of type I collagen (30 µg/mL; Gibco) and Matrigel (300 µg/mL) in serum-free DMEM for either 1 hr (for Caco-2 cells) or 2 hr (for organoid-derived epithelial cells), cell suspension was introduced into the upper microchannel (final cell density, ~1.5×10^5 cells/cm^2). After cells adhered on the surface of an ECM-coated porous membrane, culture medium was perfused through the upper microchannel at 30 µL/hr (0.02 dyne/cm^2) for up to 24 hr to form an intact cell monolayer; thereafter, the culture medium was perfused to both the upper and lower microchannels at the same flow rate. To provide peristalsis-like physical deformations on the cell monolayer, cyclic vacuum suctions that exert 10% maximum cell strain at 0.15 Hz frequency were applied via a vacuum controller (FX5K Tension instrument, Flexcell International Corporation).

To seed and grow organoid-derived primary epithelium, we followed the same protocol for preparing dissociated organoid-derived epithelial cells (See “Organoid culture”), seeded into the pre-coated chip (final cell density, ~6×10^6 cells/mL), then incubated the whole setup in a humidified CO_2 incubator at 37°C for 3 hr. After the cell attachment, we followed the same protocol described previously for the microfluidic culture.

To co-culture with endothelium in the Gut Chip (Figures 1F and S2), human capillary microvascular endothelial cells (HMVEC; final cell density at ~1.5×10^5 cells/cm^2; Lonza) pre-cultured in a conventional T75 flask were harvested and used to form a monolayer in the lower microchannel after seeding (final cell density, 1.0×10^5 cells/cm^2). After the attachment, endothelial culture medium (EBM-2 basal medium, hEGF, hydrocortisone, GA-1000 (gentamicin, amphotericin-B), FBS, VEGF, hFGF-B, R3-IGF1, and ascorbic acid; Lonza) was perfused at 30 µL/hr.

Assessment of Epithelial Morphogenesis. To test the effect of mechanical deformations on the 3D epithelial growth (Figure 1E), stretching motions were applied at 24 hr since the seeding for up to 96 hr (+Str) whereas the stretching movements were not applied in control (−Str). To assess the cessation effect of fluid flow on the formation of villi-like structure (Figure 2A), we set out two independent setups with the cessation on the apical (Figure 2A, middle) or the basolateral flow (Figure 2A, right) during the entire microfluidic cultures up to 150 hr, then phase contrast imaging was performed. To assess the cessation of flow on the pre-grown villi-like epithelium (Figure 3A), basolateral flow was ceased for up to 90 hr in the Caco-2 Gut Chip. Morphology of the epithelial structure was assessed by a phase contrast imaging. The population of proliferative cells was visualized and quantified by labeling the Ki67-positive cells. Nuclei staining was subsequently performed as a counterstaining for estimating the percentage of proliferative cells (Figure 3B). The viability of the intestinal epithelium was assessed by performing a live/dead assay. A mixture of Calcein acetoxymethyl (AM) (4 µM) and ethidium homodimer-1 (8 µM) (Figure 3C) diluted in PBS was perfused to the epithelium-grown Gut Chip at 30 µL/h in a 37ºC CO_2 incubator for 1 hr. To evaluate the inhibitory effect of basolaterally secreted compounds in Figure S4, a double-layered Caco-2 culture (i.e., two Caco-2 monolayers are adherent on both sides of the porous membrane) was conducted by seeding Caco-2 cells onto the upper microchannel first, incubating the setup for 45 min in a CO_2 incubator for the attachment, subsequently seeding dissociated Caco-2 cells onto the lower microchannel, incubating the flipped-over setup on top of a PDMS spacer in a CO_2 incubator for 45 min again, then flipping it over to run microfluidic cultures. A hybrid microfluidic device was used to introduce basolateral flow (30 µL/hr) in the Transwell containing a flat monolayer of Caco-2 or organoid-derived epithelial cells (Figures 2B middle, 2C left, and S14) by flowing fresh culture medium for 48 hr but the apical chamber was maintained static. For monitoring growth profile at various volumetric flow rates (Figures 6A and S13), we perfused culture medium into both upper and lower microchannels in the Gut Chip at flow rates of 15, 30, 70, 100, 150, and 200 µL/hr without mechanical deformations. The height of intestinal epithelium in the Gut Chip was monitored and measured by phase contrast or DIC microscopy at each given time point. To measure the height of villi, z-position was tracked using a laser scanning confocal microscopy (Leica SP5 X MP DMI-6000), at the

anchorage of the basement membrane to the villous tip or directly measured using cross-sectional images.

Disruption of the epithelial morphology was monitored by applying the known inhibitory molecules against the Wnt signaling such as dickkopf-1 (DKK-1), Wnt inhibitory factor 1 (WIF-1), secreted frizzled-related protein 1 (sFRP-1), or Soggy-1/Dickkopf-like 1 (Soggy-1/DKKL-1) (Figures 4, S6, S7, and S8). To validate the inhibitory effect of these Wnt antagonists to the growth of Caco-2 villi, human recombinant proteins of DKK-1 (rDKK-1, 100 or 500 ng/mL; R&D Systems), rWIF-1 (100 ng/mL; R&D Systems), rsFRP-1 (100 ng/mL; R&D Systems), and rSoggy-1/DKKL-1 (100 ng/mL; R&D Systems) were dissolved in the cell culture medium and perfused into the basolateral microchannel for 48 hr, respectively. In Figure 4D, anti-DKK-1 monoclonal antibodies (20 μg/mL, sodium azide-free; Abcam) were co-treated in the basolateral microchannel to block disruption of the villi-like structure by neutralizing the added rDKK-1.

Computational Simulation. A computational model was developed using COMSOL Multiphysics 4.0 based on a simplified geometry of a Gut Chip that includes the fluidic channels and the membrane surface on which the cells reside. The model included calculations for laminar flow through the channels and the transport of diluted chemical species from the cell surface due to diffusion and fluid convection. For simulating the fluid dynamics, Navier-Stokes equation assuming incompressible fluid was used, and convection of fluid was also included. As a boundary condition, the bottom of the cell channel and the membrane area were set as no-slip condition. For simulating the transport of DKK-1 and Wnt, Fick's second law was applied. The flux of the production of each molecule by the epithelium was applied based on the specific production rate (unit, mol/m^3; (Koch et al., 2009)), where the cell number per unit area was experimentally calculated. The porosity of a PDMS porous membrane (~10%) was reflected in the simulation. The concentration of DKK-1 and Wnt in the inlet of the lower microchannel was set as 0 mol/m3. The flux of each molecule from the bottom PDMS layer of the basolateral microchannel was set as zero. Mesh geometry and solver configurations were refined for solution convergence.

Morphological Analysis. Microscopic images of Caco-2 or organoid-derived primary epithelial cells in forms of a monolayer or 3D structures grown in either Transwells or Gut Chips were taken by the phase contrast microscope (Axiovert 40CFL, Zeiss) equipped with a 20× objective (0.30 Ph1; Zeiss) and a Moticam 2500 camera (Motic China Group Co., Ltd.) or a differential interference contrast (DIC) microscope (Axio Observer.Z1, Zeiss) coupled to a 20× objective (LD PlnN, 0.4 DICII; Zeiss) and a digital camera (1000×1000 8 μm pixels, EM-CCD C9100, Hamamatsu). Images were taken and processed using imaging software (Motic images plus 2.0), MetaMorph (Molecular Devices), ZEN Pro (Zeiss), or ImageJ. The villi-like microarchitecture was detected by laser scanning confocal microscopy using a 25× water immersion objective (NA 0.95) linked to the laser sources (a diode laser with 405 nm, a white light laser with 489-670 nm, or an argon laser with 488 and 496 nm) and detectors (a photomultiplier tube or HyD). Single plane or multi-plane Z-stacked confocal fluorescence images were analyzed by Leica imaging software (LAS AF; Leica Microsystems). To obtain horizontal,

vertical cross-sectional, or angled views, deconvolution (AutoQuant X, Version X3.0.1; Media Cybernetics Inc.) followed by a 2D projection process (IMARIS 7.6 F1 workstation, Bitplane Scientific Software) were performed on Z-stacked confocal fluorescence images.

For immunofluorescence microscopic analysis, epithelial cells grown in either a Transwell or a Gut Chip were fixed with 4% (w/v) paraformaldehyde (Electron Microscopy Science), permeabilized with 0.3% (v/v) Triton X-100 (Sigma), blocked with 2% (w/v) bovine serum albumin (BSA; Sigma) and washed with PBS (Ca^{2+} and Ma^{2+} free; Gibco). To fluorescently label Ki67 (Figures 3B and S9) and FZD9 (Figures 6C and S14), primary antibodies (Abcam) were diluted in 2% BSA in PBS and treated to the cells. When staining was performed in the Gut Chip, the solution was filled to both microchannels; then the upper microchannel was flowed at 30 µL/h at room temperature for 3 hr and incubated at 4°C for overnight. For the immunostaining in the hybrid chip, the solution of primary antibody was treated into the insert, incubated at room temperature for 1 hr. Secondary antibodies (DyLight 488 conjugated goat polyclonal to rabbit IgG, Abcam), also diluted in 2% BSA in PBS, was added to the microchannel under light protected at room temperature for 3 hr. For the counterstaining, samples were incubated with 4',6-diamidino-2-phenylindole dihydrochloride (DAPI; final concentration of 1.5 µM; Molecular Probe) to visualize nuclei (Figures 1B, 2C, and S10). For visualizing the F-actin, fluorescein isothiocyanate (FITC)-phalloidin (10 µM, final concentration; Sigma) was mixed with the DAPI solution and simultaneously used to stain intestinal epithelium (Figures 2C and S10).

The lesion area was defined as the percentage of the measured cell culture area where the morphology of 3D epithelial structure was destroyed by the Wnt antagonistic reactions compared to the entire available cell culture area in the Gut Chip microdevice (~0.11 cm^2). Lesion area was estimated using the ImageJ software. The height of intestinal epithelium was determined using either the DIC microscopy or the confocal immunofluorescence microscopy in conjunction with the Calcein AM (5 µM, final concentration) staining by measuring the distance of the Z position of 3D epithelium from the porous membrane to the tip of the villi-like structure (Figure S1). The height of a Caco-2 monolayer was measured by the analysis of XZ vertical cross-sectioned images using the ImageJ (Figure S10). Epithelial height represents the average maximum height of the entire epithelial layer by measuring the full height from the ECM-coated porous membrane to the villus tip.

Live cell imaging of Caco-2 epithelium was carried out by incubating the cells with the culture medium containing a cell-permeant Calcein AM (5 µM) perfused (30 µL/hr) into the upper microchannel for 30 min at 37°C. After washing with fresh culture medium (30 µL/hr) for 10 min, confocal microscopy was applied to take Z-stacks (Figure S1). A contour of the 3D epithelial structure was visualized using a fluorescence dye (5 µL/mL; CellMask, Molecular Probe) targeting the plasma membrane of epithelium (Figures 1C and 5C).

Effect of FZD9 neutralization on the 3D morphogenesis was assessed by introducing the anti-FZD9 antibodies (20 µg/mL; sodium azide-free, Abcam) to the Caco-2 epithelium grown in a Gut Chip device. Culture medium containing antibodies was perfused through to both upper and lower microchannels at 30 µL/hr for up to 24 hr. Morphology of the 3D structure was monitored using a DIC microscope (DMi8, Leica).

Quantification of secreted DKK-1. Secretory DKK-1 by the Caco-2 cells was quantified using an enzyme-linked immunosorbent assay (ELISA) kit that targets human DKK-1 (Quantikine ELISA, R&D Systems) according to the manufacturer's protocol. Culture medium collected from both apical and basolateral sides of the Transwell that contains a Caco-2 cell monolayer was used for the DKK-1 quantification.

Assessment of epithelial barrier function. The barrier function of the intestinal epithelial layer was measured by monitoring transepithelial electrical resistance (TEER). TEER was measured by using Ag/AgCl electrodes connected to an ohm meter (87V Industrial Multimeter, Fluke Corporation). Normalization of TEER was performed following an equation below. TEER = $(\Omega_t - \Omega_{blank})/(\Omega_0 - \Omega_{blank})$, where Ω_t is resistance at the measured time point since the onset of the experiment, Ω_{blank} is a resistance without the epithelium, and Ω_0 is resistance at the onset time point.

Genetic Analysis. Expression profile of the genes related to human Wnt pathway was analyzed by the quantitative real time polymerase chain reaction (qPCR) following the protocol provided by the manufacturer for preparing cDNA (Cells-to-cDNA II Kit, Life Technologies) and running multiplexed qPCR (TaqMan Array Human WNT Pathway 96-well Plate, ThermoFisher Scientific) that targets pre-arrayed 92 Wnt related genes (APC, AXIN1, AXIN2, BTRC, CSNK1A1, CSNK1D, CSNK1G1, CSNK1G2, CSNK1G3, CSNK2A1, CSNK2A2, CSNK2B, CTNNB1, CTNNBIP1, CXXC4, DACT1, DKK1, DKK2, DKK3, DKK4, DVL1, DVL2, DVL3, EP300, FBXW11, FGF4, FOXN1, FRAT1, FRAT2, FRZB, FZD1, FZD2, FZD3, FZD4, FZD6, FZD7, FZD8, FZD9, FZD10, GSK3A, GSK3B, KREMEN1, KREMEN2, LEF1, LRP5, LRP6, MYC, NKD1, NLK, CBY1, PITX2, PORCN, PPP2CA, PPP2R1A, PYGO1, PYGO2, RHOU, SENP2, SERP1, SERP2, SERP4, SERP5, SLC9A3R1, TCF7, TCF7L1, TCF7L2, TLE1, TLE2, TLE3, TLE4, TLE6, WIF1, WISP1, WNT1, WNT10A, WNT10B, WNT11, WNT16, WNT2, WNT2B, WNT3, WNT3A, WNT4, WNT5A, WNT5B, WNT6, WNT7A, WNT7B, WNT8A, WNT8B, WNT9A, WNT8B). As a control, Caco-2 cells grown in a static Transwell for two weeks were used. As test groups, Caco-2 cells cultured at three different flow rates (30, 100, and 200 μL/hr) without mechanical deformations were independently harvested. Fold increase of each target gene was estimated by comparing the gene expression level in the test groups (i.e., Gut Chips) to the one in control (i.e., Transwells). Two independent batches were performed with two technical replicates for qPCR analysis. Due to the limited sample amount, we merged two technical replicates in a single tube. Results were analyzed using the standard R statistical software.

Quantification and statistical analysis. All results and error bars in this article are represented as a mean ± standard error (S.E.M.). For statistical analyses, a one-way analysis of variance (ANOVA) with Tukey-Kramer multiple comparisons test was performed using GraphPad InStat software, version 3.10 (GraphPad Software Inc.). Differences between groups were considered statistically significant when $p<0.05$. Microscopic images were recorded at more than ten different random locations in either Transwells or Gut Chips from at least two independent replicates at each time point, and representative images were displayed in the Figures.

SUPPLMENETAL REFERENCES

Kim, H.J., Huh, D., Hamilton, G., and Ingber, D.E. (2012). Human gut-on-a-chip inhabited by microbial flora that experiences intestinal peristalsis-like motions and flow. Lab Chip *12*, 2165-2174.

Koch, S., Capaldo, C.T., Samarin, S., Nava, P., Neumaier, I., Skerra, A., Sacks, D.B., Parkos, C.A., and Nusrat, A. (2009). Dkk-1 inhibits intestinal epithelial cell migration by attenuating directional polarization of leading edge cells. Mol. Biol. Cell *20*, 4816-4825.

Rajan, A., Vela, L., Zeng, X.-L., Yu, X., Shroyer, N., Blutt, S.E., Poole, N.M., Carlin, L.G., Nataro, J.P., and Estes, M.K.J.M. (2018). Novel Segment-and Host-Specific Patterns of Enteroaggregative Escherichia coli Adherence to Human Intestinal Enteroids. *9*, e02419-02417.

Sato, T., Stange, D.E., Ferrante, M., Vries, R.G., Van Es, J.H., Van Den Brink, S., Van Houdt, W.J., Pronk, A., Van Gorp, J., and Siersema, P.D. (2011). Long-term expansion of epithelial organoids from human colon, adenoma, adenocarcinoma, and Barrett's epithelium. Gastroenterology *141*, 1762-1772.

Saxena, K., Blutt, S.E., Ettayebi, K., Zeng, X.-L., Broughman, J.R., Crawford, S.E., Karandikar, U., Sastri, N.P., Conner, M.E., and Opekun, A. (2015). Human intestinal enteroids: a new model to study human rotavirus infection, host restriction and pathophysiology. J. Virol., JVI. 01930-01915.

Sick, S., Reinker, S., Timmer, J., and Schlake, T. (2006). WNT and DKK determine hair follicle spacing through a reaction-diffusion mechanism. Science *314*, 1447-1450.